BIAXIAL RESTRAINT OF AXIALLY LOADED STEEL CORES

by

Brett Jay Raddon

A thesis submitted to the faculty of
The University of Utah
in partial fulfillment of the requirements for the degree of

Master of Science

Department of Civil and Environmental Engineering

The University of Utah

December 2010

The University of Utah Graduate School

STATEMENT OF THESIS APPROVAL

The thesis of **Brett Jay Raddon**

has been approved by the following supervisory committee members:

Chris P. Pantelides	, Chair	**10/27/2010** Date Approved
Lawrence D. Reaveley	, Member	**10/27/2010** Date Approved
Pedro Romero	, Member	**10/27/2010** Date Approved

and by **Paul J. Tikalsky**, Chair of the Department of **Civil and Environmental Engineering**

and by Charles A. Wight, Dean of The Graduate School.

ABSTRACT

The results from the testing of six short steel specimens are presented in this thesis to represent a portion of a full scale specimen of a solid steel round core confined by a steel tube, termed here as a biaxial restrained axially loaded steel core. The biaxial restrained axially loaded steel core is a first step in the development of a potentially effective restrained core for a Buckling Restraining Brace (BRB). In addition, four solid steel round bars are tested as controls to compare with the six short scale restrained specimens.

Three objectives were explored in this study of the compressive behavior of a sleeved steel core. The first objective is to determine if a steel core restrained by a steel sleeve with a gap in between will have increased compressive properties and resist buckling. The second objective is to determine if a steel core restrained by a steel sleeve with a gap can increase the energy dissipation of the system compared to a solid steel round bar with the same dimensions. The third objective is to determine if lead foil placed between the two elements would act as a friction reducing mechanism, thereby minimizing the amount of axial load that would be transferred to the steel sleeve.

The short steel specimens gained an increase of 45% to 48% in compressive strength compared to a core without a restraining sleeve. Energy dissipation increased with the sleeved compression members. Energy dissipation for the short steel specimens

increased 85% to 246%. Lead was determined to be an appropriate intermediate material for applications requiring high early energy dissipation.

The results of this study on six sleeved compression members and four solid steel round bars was a success and the objectives of the study were achieved.

TABLE OF CONTENTS

LIST OF FIGURES

LIST OF TABLES

ACKNOWLEDGEMENTS

I would like to thank Dr. Larry Reaveley, Dr. Chris Pantelides and Dr. Pedro Romero for their guidance, patience and determination to help me to achieve my educational goals. They always had time to meet with me and answer my questions about my research. Without the special effort I feel was given to me I could not finish this thesis.

I would like to thank Mark Bryant for his help and patience throughout the testing phase of the research and for the long talks about football. He helped me keep things in perspective and keep my feet on solid ground.

I would also like to also thank all those who taught me how to use equipment, reduce data, and other tasks. These individuals include, but are not limited to, Clayton Burningham, Stephan Woll, Timothy Garfield, Michael Gibbons, Adam Olsen and Michael Rigby.

Finally, I would like to also thank my parents, family and friends for their continued support and words of encouragement. I would like to express my deep appreciation for my wife, Jana, and my two kids, Jovie and Brock. It is always appreciated to be reminded what is most important.

1. INTRODUCTION

1.1 General

Structural engineers are faced with many different challenges when designing structures, but in seismic regions the challenges are amplified. An earthquake may produce a wide range of dominant frequencies within a specific ground motion. When the fundamental period of a structure coincides with the dominant period of an earthquake, the forces generated in the structure due to the input earthquake energy will be amplified resulting in greater damage. To reduce these amplified seismic forces, engineers sometimes try to increase the natural period of the structure to avoid resonance. However, this can only be achieved for certain structures amenable to base isolation. Another method of counteracting the amplified seismic forces is to employ mechanisms that dissipate energy.

In the early 1980s a Japanese company developed a device to dissipate energy. The device, called "Unbonded Brace," utilized a steel yielding core surrounded by a concrete filled structural steel tube. It is called an "unbonded brace" because it utilizes an unbonded layer to separate the steel core from the concrete restraint. This device dissipates energy by allowing the core to yield in tension and resist buckling with the confined concrete inside the steel tube. This allows the core to yield without buckling and thereby increase the ductility of the structural system. This type of energy dissipation is called hysteretic energy dissipation when it results from cyclic loading.

The results from testing six short steel specimens are presented in this thesis to represent a portion of a full scale specimen of a solid steel round core confined by a steel tube, termed here a biaxial restrained axially loaded steel core. The biaxial restrained axially loaded steel core is a first step in the development of a potentially effective restrained core for a Buckling Restraining Brace (BRB). In addition, four solid steel round cores were tested as controls to compare with the six restrained specimens. A description of the testing apparatus, the results of the experiments, discussion and recommendations are provided in this thesis. More research will be needed to explore how these concepts can be utilized in improving the seismic performance of structural systems utilizing biaxially restrained steel round cores confined with steel tubes.

1.2 Objectives

Three objectives were explored in this study of the compressive behavior of a sleeved steel core. The first objective is to determine if a steel core restrained by a steel sleeve with a gap in between will have increased compressive properties and resist buckling. The second objective is to determine if a steel core restrained by a steel sleeve with a gap can increase the energy dissipation of the system compared to just a solid steel round bar with the same dimensions. The third objective is to determine if lead foil placed between the two elements in the gap between the steel core and steel tube would act as a friction reducing mechanism, thereby minimizing the amount of axial load that is transferred to the outer sleeve. This could be achieved if the core were allowed to slide along the surface of the steel pipe. Radial expansion of the inner core would then be restrained by the outer sleeve. In that case, it is anticipated that the steel sleeve would be more effective in resisting buckling of the steel core.

2. LITERATURE REVIEW

2.1 Introduction

The purpose of this literature review is to gain a background and an understanding of the concept of sleeved compression members. This is done by first introducing two of the patents related to sleeved compression members and the claims made in each patent. Secondly, an understanding of how steel behaves under compression is sought. Finally, the types of applications which use sleeved compression members to include buckling restraining brace technology (BRB) and carbon fiber wrapped solid steel round cores are explored.

2.2 Patents on Sleeved Compression Member Design

Benne N. Sridhara (1993) filed a patent describing a sleeve column compression member. This patent claims a compression member, either in several short segments or in one segment, with a sleeve large enough to leave some space around, so that the sleeve resists bending forces only as a buckling prevention member for compression type elements such as cores. Euler's buckling load equation for a pinned connection at both ends is mentioned in the description of the patent as:

$$P_{cr} = \frac{\pi^2 EI}{l^2}$$

where P_{cr} is the critical buckling load, E is the modulus of elasticity, I is the least moment of inertia for the cross section, and l is the unbraced length of the member. According to Sridhara, compression members would have to have an increased modulus of elasticity or moment of inertia to gain more capacity. His invention increases the capacity of a compression member without increasing the amount of material used by supplying an outer shell to constrain the core from buckling. Also since the compression member does not have to resist any bending, the material yield strength used can be reduced. This patent though important to this thesis (it uses a steel core with a steel restraining sleeve without filler concrete) does not envision any type of material be placed between the core and restraining sleeve to decrease friction between the compression member and the sleeve.

Another United States patent by Sugisawa et al. (1994) describes a Buckling-Restraining Bracing Member. The invention explains how the manufacturing of buckling-restraining braces (BRB) is difficult to produce because of the time restrictions attributed to the casting and curing of the concrete. Traditionally, BRB technology has consisted of a yielding core restrained by a concrete filled steel tube. The steel tube would have to be raised vertically to place the concrete inside and a nonstick coating would have to be used to separate the yielding core from the concrete as well. The patent by Sugisawa et al. (1994) does away with the use of concrete and uses steel to restrict the yielding core from buckling. Several different setups are claimed in the patent to include a steel yielding pipe restrained by a steel pipe, and also to include a stick preventing coating separating the two members.

2.3 Steel Compression

Sparse information is available regarding the compression resistance of solid steel shapes. Nevertheless the information found on the subject gives a basic understanding of the behavior of steel in compression.

Galambos (1965) conducted a study of 27 round steel bars, made of A514 steel or structural carbon steel, with diameters ranging from 2.75 in. to 7.5 in. The yield stress for the bars ranged from 121,000 to 128,000 psi with moduli of elasticity ranging from approximately 29,000,000 to 31,000,000 psi. Each bar was compressed axially and tested until failure. The data collected from these tests were compared to theoretical predictions. Theoretical values were predicted using the tangent modulus theory, a theory where a line tangent to the critical point becomes the tangent modulus of elasticity and used in Euler's critical buckling load equation by replacing the modulus of elasticity, to predict failure of the solid steel round bars. According to Galambos (1965), excellent correlations between theoretical and experimental values of the load deformation behavior of the axially loaded columns were achieved. Experimental loads for buckling were 12% to 24% below the theoretical load.

Sennah et al. (2004), presented findings on six solid round steel bars, three non-relieved steel and three stress relieved steel. Test specimen dimensions were 4.3 in. in diameter and 30 in. long. Specimens were made of Grade 50 steel with actual yield strength of 57,700 psi and a modulus of elasticity of approximately 26,000,000 psi. Specimens were positioned in a compression machine with a pinned condition on the top and fixed condition on the bottom. The specimens were loaded monotonically until failure. Failure was determined when visual buckling occurred. Each specimen failed in

a typical buckling hinged-fixed manner. An effective length factor (*k*) of 0.7 for this condition was used in failure load equations to determine theoretical failure loads from the AISC-LRFD Specification (1993). The AISC-LRFD Specification equation for the theoretical failure load underestimates the compressive resistance by an average of 13% for the non-stressed-relieved solid round steel bar and 24% for the stress-relieved solid round steel bars.

In his master's thesis, Mull (1999) describes tests on 40 solid round steel bars. Bar sizes range from 1.25 in. to 2.25 in. in diameter and 22 in. to 56.5 in. in length. Yield strengths for the specimens used ranged from approximately 46,000 to 57,000 psi all with a modulus of elasticity of approximately 29,000,000 psi. The setup was unlike Sennah (2004) in that the specimens had both ends pinned. Mull cut notches at the top and bottom of each specimen and inserted a centering pin. The centering pin allowed for the specimen to be free of moments at the ends. Results for 8 specimens with a 2 in. nominal diameter and varying lengths show that the AISC-LRFD Specification (1993) theoretical load failure equation overestimates on average 2% more load compared to the experimental load at failure. Mull also analyzed the solid steel round bars using finite element software. The software showed a theoretical failure load for the solid steel round bars to be on average 18% lower than that of the experimental failure load.

2.4 Sleeved Compression Member Studies

Sleeved compression member studies include buckling restraining braces and carbon fiber wrapped steel.

Kalyanaraman et al. (1998) explain the idea behind Sridhara's patent. A core resists the axial load and a sleeve prevents the core from buckling; this prevents global

buckling of the core and sleeve. It is stated that a material is placed between the core and sleeve to prevent axial load from being applied to the sleeve. Since no axial load is applied to the sleeve, it is assumed by Kalyanaraman et al. (1998) that buckling of the sleeve is nearly equal to the Euler buckling strength of the sleeve allowing the core to experience strains well beyond its yield strain.

Ekiz and El-Tawil (2008) performed a study of 22 solid steel round bars wrapped with a carbon fiber reinforced polymer composite jacket with varied end conditions and sandwiched between two different types of core material, mortar and PVC. The objective of the study was to determine whether any increase in flexural capacity of steel during compression of the core material with the carbon fiber jacket attached would occur. Some of the specimens were tested without any bond between the carbon fiber jacket and the core material. It was determined that the specimens performed better without bond between the carbon fiber jacket and the core. The researchers found improvements in flexural strengthening of the steel bars when the core material was wrapped with the carbon fiber jacket. It was determined that the steel core could reach yield if the appropriate amount of core material and number of layers of carbon fiber composite were used. In seismic applications it is desirable for the steel to yield and deform prior to buckling of the composite system to avoid catastrophic failure.

3. SPECIFIC SCOPE

3.1 Purpose

The purpose of this research is to (1) determine if the compressive strength of a steel core is increased by restraining the core from expanding; (2) determine if the energy dissipation of the steel sleeved specimens increase compared to the solid steel round bars; and (3) compare the performance characteristics of the specimens prepared using lead as an intermediate material between the compressed core and the restraining sleeve.

3.2 Sleeved Core Specimen and Solid Steel Round Bar Details

This portion of the research is comprised of six different test specimens at two different lengths, three short specimens with a 12 in. long core and three long specimens with a 24 in. long core. Fig. 1 is a representation of the specimens. Specimens are comprised of three main parts: (1) a 2 in. nominal diameter core made of solid A36 steel round bars; the core will resist the entire compressive load, (2) a restraining sleeve made of 2 in. inside diameter nominal Grade B steel pipe conforming to ASTM A106 for seamless carbon steel pipe; the pipe resists outward expansion of the core under axial load and is cut at a length approximately 0.5 in. longer than the yielding core, and (3) lead foil situated in the gap between the core and the restraining sleeve.

The thickness of the foil is approximately 0.015 in. The lead foil reduces friction between the core and the restraining sleeve. Four specimens were constructed using a

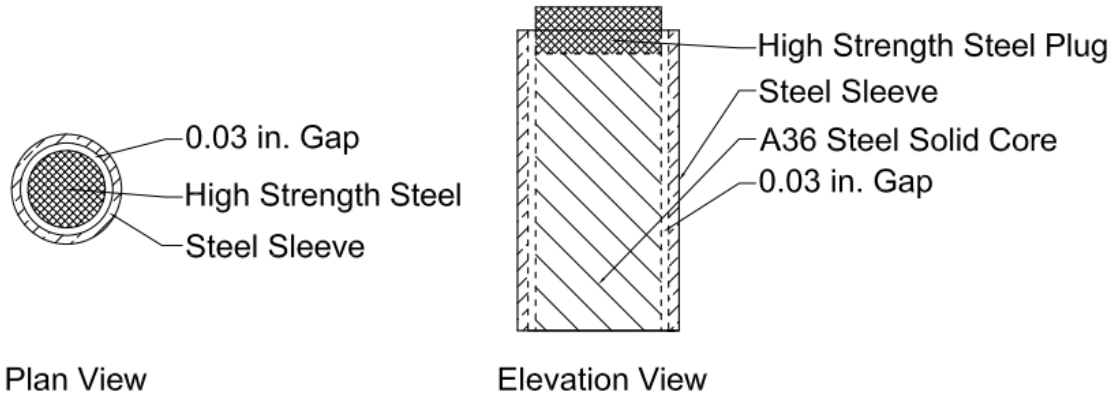

Figure 1: Plan and elevation view of specimens

lead foil and two specimens were tested without any intermediate material. Table 1 describes each specimen in detail.

For comparison with the six sleeved specimens, four additional tests on solid steel round bars are presented in this thesis. The solid steel round bars are made of ASTM A36 steel, the same as the cores of the six sleeved specimens. The solid steel round bars

Table 1: Sleeved specimen dimensions

Specimen Identification	With or Without Lead	Core Diameter (in.)	Core Length (in.)	Pipe Inside Diameter (in.)	Pipe Outside Diameter (in.)	Pipe Length (in.)	Gap Size* (in.)
S12W1	No Lead	2.007	12.14	2.06	2.38	12.5	0.027
S12L1	Lead	2.003	12.14	2.06	2.38	12.5	0.029
S12l2	Lead	2.005	12.14	2.06	2.37	12.5	0.028
L24W1	No Lead	2.005	24.00	2.06	2.37	24.5	0.027
L24L1	Lead	2.004	24.00	2.06	2.36	24.5	0.028
L24L2	Lead	2.002	24.00	2.06	2.38	24.5	0.029

* 1/2 of the difference between the pipe inside diameter and the core diameter

are used as reference to compare if an increase in compressive strength has occurred. Table 2 describes each solid steel round bar in detail.

Table 2: Solid steel round bar dimensions

Core Diameter (in.)	Core Length (in.)
2.0	12.0
2.5	12.1
2.0	24.0
2.5	24.0

4. TEST SETUP

4.1 Materials

4.1.1 A36 steel. The cores of the short 12 in. and long 24 in. specimens and the four solid steel round bars are made of A36 steel. This type of steel was selected for the core because of the yielding properties associated with A36 steel. A36 steel is defined by ASTM A36/A36M – 08 as "Carbon Structural Steel." It is mild steel for general purpose work and easily welds. The tensile strength of A36 steel ranges from 58,000 to 80,000 psi and has nominal yield strength of 36,000 psi. Actual tested values of the yield strength in compression ranged from approximately 42,000 psi to 48,000 psi.

4.1.2 1215 cold roll steel. 1215 steel conforms to ASTM A29 and A108 for cold rolled steel. It is used as a high strength plug attached to the testing apparatus as shown in Fig. 1. This type of steel was selected for its high strength. The steel has tensile yield strength of 75,000 psi and an ultimate tensile strength of 87,000 psi.

4.1.3 Hot finished seamless carbon steel pipe. Steel pipe was used for the outer sleeve and the biaxial constraint of each sleeved specimen. This pipe conforms to ASTM A106/A106M – 08 for "Seamless Carbon Steel Pipe for High-Temperature Service." The pipe was made from grade B steel. The yield strength and ultimate tensile strength for grade B steel is 35,000 psi and 60,000 psi, respectively.

4.1.4 Lead. Lead is used as in intermediate material between the inner core and the outer sleeve for four of the specimens. Lead was selected because of the unique

properties attributed to it for reducing friction and binding between the inner core and the outer pipe sleeve during compression. Lead is highly malleable with low yield strength.

4.2 Apparatus

Fig. 2 is a representation of the apparatus used in testing the short 12 in. and long 24 in. specimens. The specimens were sandwiched between two 1in. thick steel plates. A 1.5 in. long and 2 in. diameter 1215 high strength steel plug was tack welded to the top 1 in. plate. The steel plug projects downward into the external sleeve, and abutted the various cores. The steel pipe sleeves were designed to be approximately 0.5 in. longer than the core. This was done to ensure that the core was completely inside the sleeve for its whole length and to avoid any bulging of the core outside of the sleeve at the ends. The high strength steel plug would not yield before the core and is assumed not to bulge beyond the Poisson's effect and add stress to the sleeve.

Hinged-fixed end conditions were used for testing of all the specimens. This was accomplished by using a circular hemispherical bearing plate on the top of the testing

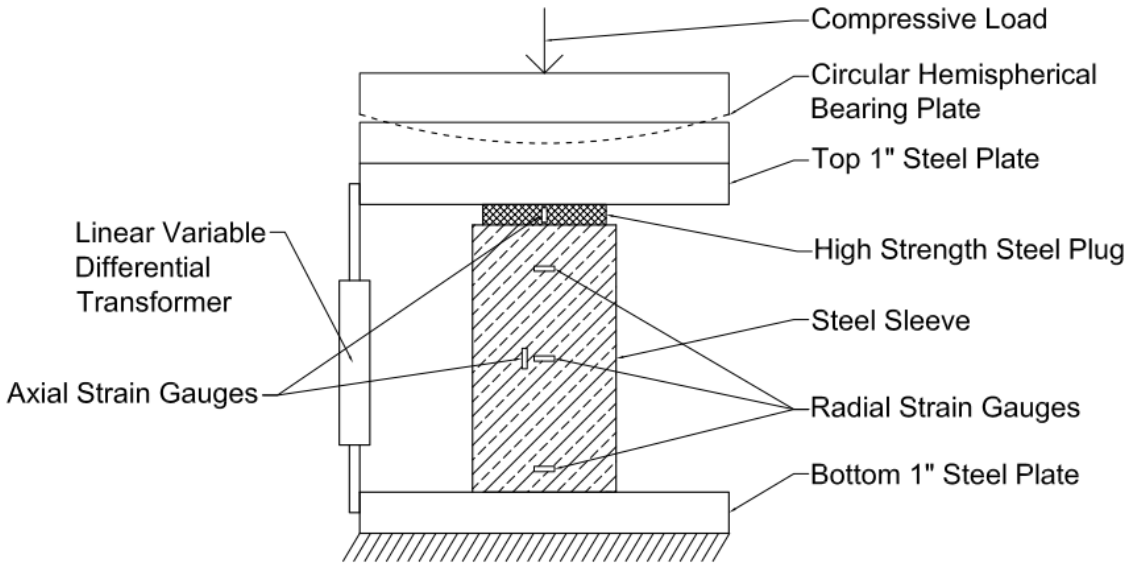

Figure 2: Testing and instrumentation apparatus

apparatus for a relatively, due to friction, hinged end condition and a flat plate on the bottom for a relatively fixed end condition.

Three strain gauges were attached to the specimen. The strain gauges were applied to the sleeve of each specimen and positioned at approximately the mid-height and 1 in. from the bottom and top of the core. Data collected from three strain gauges indicate when the core engages the sleeve and the radial strain at these locations.

Two strain gauges were used to measure axial strain. One gauge was placed on the sleeve of the specimen at mid-height to measure the axial strain applied to the steel sleeve. The second strain gauge was placed on the steel plug to measure the axial strain and to indicate whether or not the steel plug yielded.

Axial displacement was measured using a Linear Variable Differential Transformer (LVDT) and this was used to calculate overall axial strain. The LVDT was attached to the top and bottom 1 in. steel plates as shown in Fig. 2. The strain of the steel plug was subtracted from the LVDT strain to more accurately describe the strain of the core of the specimen.

4.3 Testing Equipment and Protocol

An Instron compressive machine with a load capacity of 400,000 pounds was used for all compression tests. The software allowed a protocol to be established with a head displacement of 0.02 in. per minute. This load rate was selected to ensure a static type of loading. For this research, the Instron collected only force data for all specimens. The data collection rate was 10 points per second. A Vishay data collector unit was used to collect data from all four strain gauges and the LVDT. The data collection rate was 10

points per second as well. Both machines were started at essentially the same time to be able to compare the data according to time.

4.4 Failure Criteria

Failure of a specimen was determined when visual buckling occurred for both the sleeved and unsleeved specimens. Fig. 3 is a picture of sleeved specimen S12L1 in a buckled configuration.

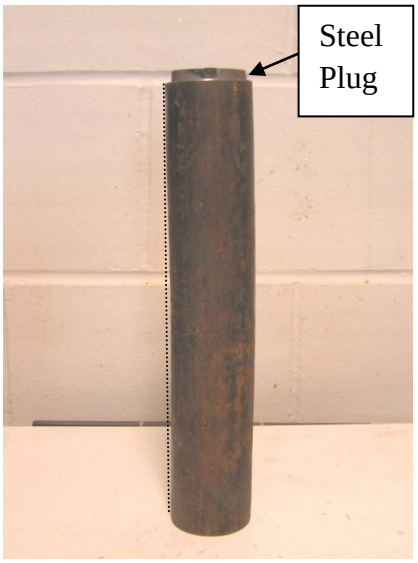

Figure 3: Buckled S12L1 sleeved specimen

5. TEST RESULTS

5.1 Introduction

The various specimens that are listed in Tables 1 and 2 were tested according to the protocol described in Section 4. The results are described in this chapter.

Solid steel round bars with approximately 2 in. and 2.5 in. diameters were compressed for comparison to the sleeved specimens. The lengths of the solid steel round bars were also varied to be either 12 in. or 24 in. Table 2 describes each solid steel round bar in detail.

All six sleeved compression members are comprised of a 2 in. diameter mild steel core and 2 in. nominal standard seamless steel pipe as the outer sleeve. The design of the steel sleeved specimens allowed for a 0.030 in. gap between the core and the pipe sleeve all the way around the core. A 0.015 in. thick sheet of lead was inserted into the gap of four specimens, two for each specimen length. This insertion of the lead sheet leaves a 0.015 in. gap all the way around the core. For actual dimensions of the steel sleeved specimens refer to Table 1 and Fig. 1.

5.2 Modulus of Elasticity of Steel in Compression

The modulus of elasticity is the relationship of the stress and strain before yielding. The modulus of elasticity for steel in tension is well known and is assumed to be approximated 29,000,000 psi. It is important not to use the tensile modulus of

elasticity for compression because during a tensile test the cross sectional area of the steel will decrease due to Poisson's effect; the cross sectional area of steel during a compression test will increase. The increase in the cross sectional area for compression affects the stress of the steel altering the modulus of elasticity. Due to a paucity of information dealing with the modulus of elasticity for steel in compression, preliminary compression tests for two solid steel round bars with nominal dimensions of 2 in. diameter and two different lengths of 18 in. and 24 in. were performed. The Instron compression machine and an extensometer, a device to measure strain, were used to determine the stress and the strain of the solid steel bars. Fig. 4 is the stress/strain relationship of the two tests.

Using the Microsoft Excel trend line function, which uses the least squares method to determine a best fit line, a determination of the modulus of elasticity for compression of steel was found to be approximately 32,000,000 psi. The 18 in. long solid

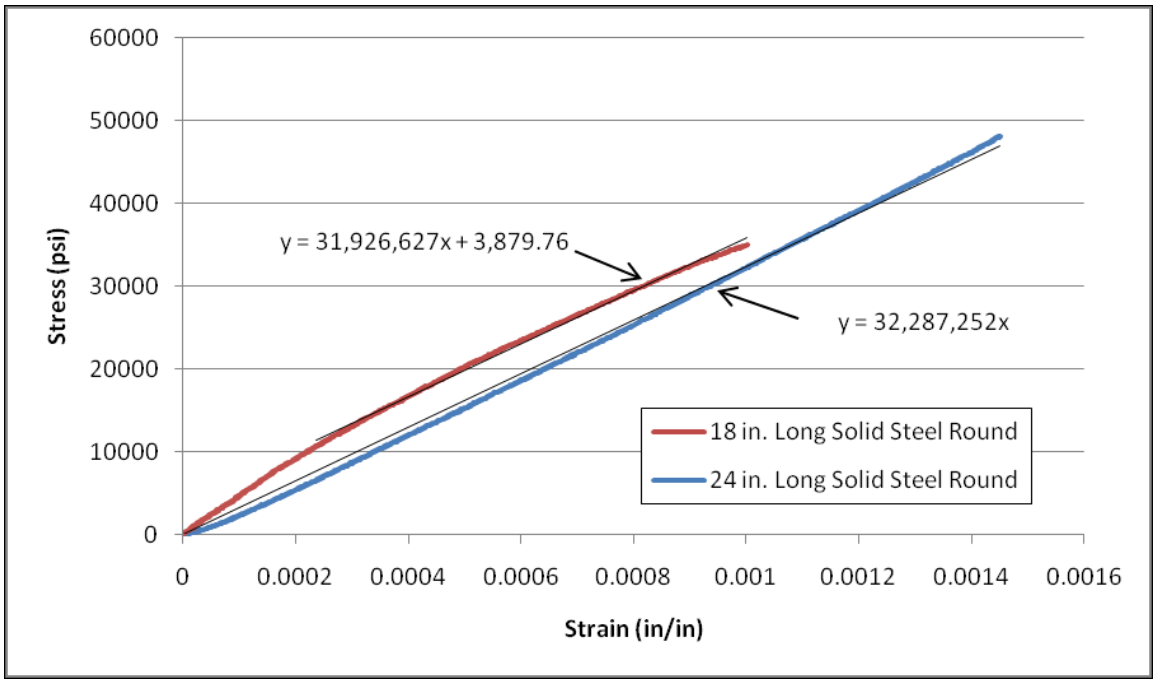

Figure 4: Determination of modulus of elasticity for steel in compression

steel round bar experienced some seating probably due to a slight unevenness in the surfaces of the compression areas. Through further testing of the solid steel round bars it was determined that the lengths of the specimens were not slender and would fail in the inelastic range negating the use of the modulus of elasticity in any calculations to predict buckling. The modulus of elasticity is useful in calculating a lower and upper bound of gap size.

5.3 Solid Steel Rounds Bars

The compression of solid steel round bars without a constraining sleeve was conducted in this portion of the research. The information gathered from the solid steel round bars was used to find the tangent modulus of elasticity of the steel and to make a comparison of the actual and predicted buckling loads. A total of four solid steel round bars were compressed, two 2 in. diameter round bars, one short and one long; and two 2.5 in. diameter round bars, also one short and one long.

A hinged-fixed end condition was applied to the solid steel round bars. This was achieved by placing a circular hemispherical bearing plate on top of the specimen and fixing the bottom of the specimen. The k-value for a hinged-fixed end condition is 0.7 which is used throughout this thesis. Slenderness is calculated using Equation 1.

$$Slenderness\ Ratio = \frac{kl}{r} \tag{1}$$

where *k* is the column effective length factor, *l* is the length of the specimen and *r* is the radius of gyration. The radius of gyration for solid round cylinders is equal to half of the radius. For design of axially loaded steel members, if the slenderness ratio is greater than 200 then the member is considered too slender to carry compression and redesign is required because the member will fail by buckling in the elastic range and not yield.

Slenderness ratios for the solid steel round bars are presented in Table 3. The slenderness ratios found for the solid steel round bars presented in this thesis are all below 50, which is a good indication that the specimens will fail by buckling in the inelastic region.

Because the specimens will fail in the inelastic region, elastic buckling equations cannot be utilized to predict buckling failure. According to Timoshenko and Gere (1961) the inelastic critical buckling load or P_{cr} can be found by replacing the modulus of elasticity in the elastic critical buckling load equation with the tangent modulus of elasticity. Equation 2 shows the inelastic critical buckling load:

$$P_{cr} = \frac{\pi^2 E_t A}{\left(kl/r\right)^2} \tag{2}$$

where P_{cr} is the critical buckling load, E_t is the tangent modulus of elasticity, A is the cross-sectional area and kl/r is the slenderness ratio.

The tangent modulus of elasticity is not easily defined outside of the proportional limit because stress and strain do not have a linear relationship. Fig. 5 is a representation of a compression test diagram. Point C corresponds to the critical condition of the stress-strain relationship, then line CC″ is the initial modulus of elasticity and line CC' is the tangent modulus of elasticity. Timoshenko and Gere (1961) fit a curve on a plot representing the tangent modulus using the slenderness ratio and the critical stress of an

Table 3: Experimental and theoretical values for critical load of solid steel round bars

Length (in)	Diameter (in)	kl/r	Experimental P_{cr} (lb)	σ_{cr} (psi)	E_t (psi)	Theoretical P_{cr} (lb)	% Difference
12	2.5	13.4	274714	48500	887647	238074	13%
12	2	16.8	180275	48000	1372651	150796	16%
24	2.5	26.9	215720	42500	3111342	208621	3%
24	2	33.6	144911	42000	4804278	131947	9%

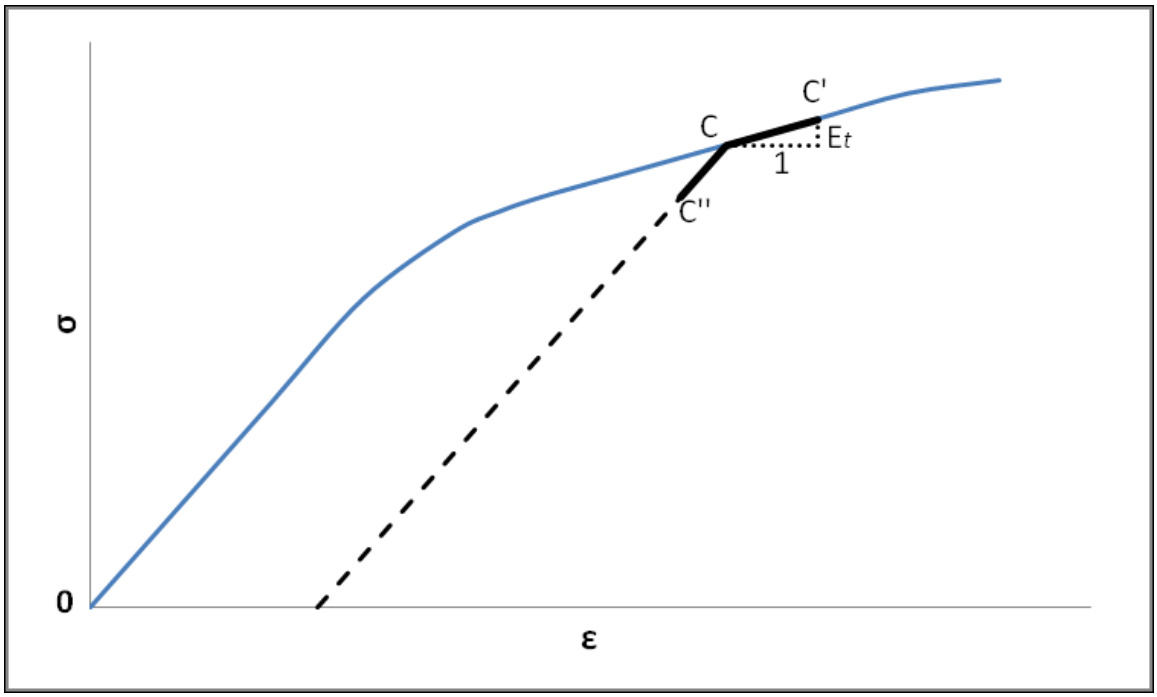

Figure 5: Tangent modulus diagram

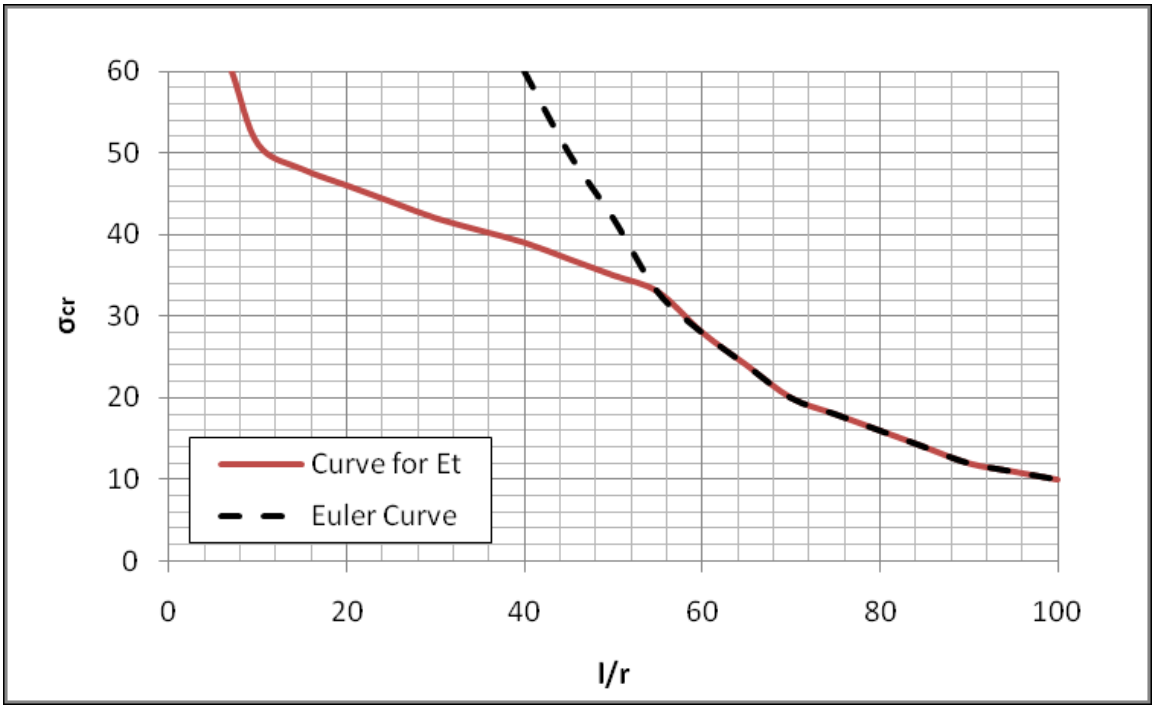

Figure 6: Euler curve and tangent modulus curve

axially loaded member. Fig. 6 is a plot similar to Timoshenko's plot. The Tangent Modulus curve and Euler's curve converge in the elastic range and diverge in the inelastic range. The plot can be utilized regardless of the shape of the cross section. The curve also shows that for long slender members the critical buckling stress follows Euler's curve and, as the member becomes shorter, it follows the curve for the tangent modulus. Values for the critical stress of the four solid steel round bars tested are found in Table 3.

The tangent modulus can then be obtained using the values found for the critical stress using Equation 3.

$$E_t = \frac{\sigma_{cr}\left(kl/r\right)^2}{\pi} \tag{3}$$

The tangent modulus can now be used to predict the critical buckling load for the four solid steel round bars. The values for the predicted buckling loads are found in Table 3 and are compared to the actual buckling loads found through experimentation.

The four solid steel round bars were placed in the Instron compression machine and were loaded at a rate of 0.02 in. per minute. Load data were recorded using the Instron software. Vishay data collection software was used to collect data from a Linear Variable Differential Transformer (LVDT) attached to the testing apparatus to measure displacement. Figs. 7, 8, 9, and 10 are pictures of the four solid steel round bars after testing.

All four solid steel round bars failed in a hinged-fixed manner in a nonlinear buckling mode. The values of the experimental critical buckling load are shown in Table 3. The percent difference was also calculated to show the difference between the

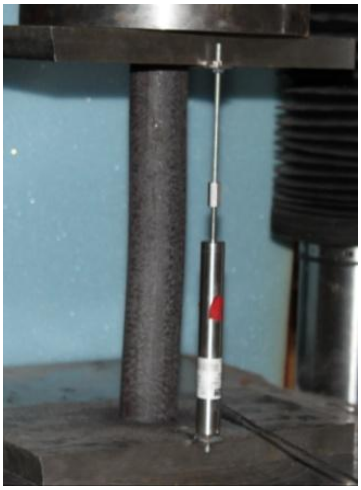

Figure 7: 2 in. Short solid steel bar

Figure 8: 2 in. Long solid steel bar

Figure 9: 2.5 in. Short solid steel bar

Figure 10: 2.5 in. Long solid steel bar

theoretical and experimental values. This is useful in predicting values of critical buckling loads for different slenderness ratios. The critical buckling load for the long specimens was 3% to 9% higher than the theoretical values calculated. The critical buckling load for the short specimen was 13% to 16% higher than the theoretical values. These values correspond nicely with percent differences between theoretical and experimental values found by Galambos (1965), Sennah et al. (2004), and Mull (1999).

Figs. 11 and 12 show the stress versus strain plots of the solid steel round bars. These two plots show a difference in the behavior of shorter members (Fig. 11) compared to longer members (Fig. 12). The 24 in. long solid steel round bars buckled during yielding before strain hardening took place in a pronounced buckled shape; the 12 in. long solid steel round bars failed in a moderate buckled shape considerably after strain hardening. This helps explain the variance of the differences observed between experimental and theoretical values of the critical buckling load.

The compression tests of the solid steel round bars were important because they allow for comparisons to be made for the increase in axial stress obtained by restricting compressive members from buckling with the use of the outer sleeve. The 2 in. diameter solid steel round bars are used as the standard for comparison and the 2.5 in. diameter bars are used to determine a range of diameters. One can also determine the general stress/strain shape and characteristics of steel in compression which are not generally found in their literature.

It can be seen from Figs. 11 and 12 that the yield strength of the steel for the 2 in. diameter and the 2.5 in. diameter solid steel round bars was different. This is due to the range of yield stresses ASTM A36 steel can qualify. The steel used in the 2 in. diameter and 2.5 in. diameter solid steel round bars did not come from the same lot or batch.

5.4 Lower and Upper Boundary of Gap Distance

Information gathered from the modulus elasticity of compressed steel and the solid steel round bars was used to find a lower and upper boundary for the gap distance between the solid steel core and the constraining sleeve. If the gap is too small, binding between the core and the sleeve will occur before the core yields, due to Poisson's effect. If the gap is too

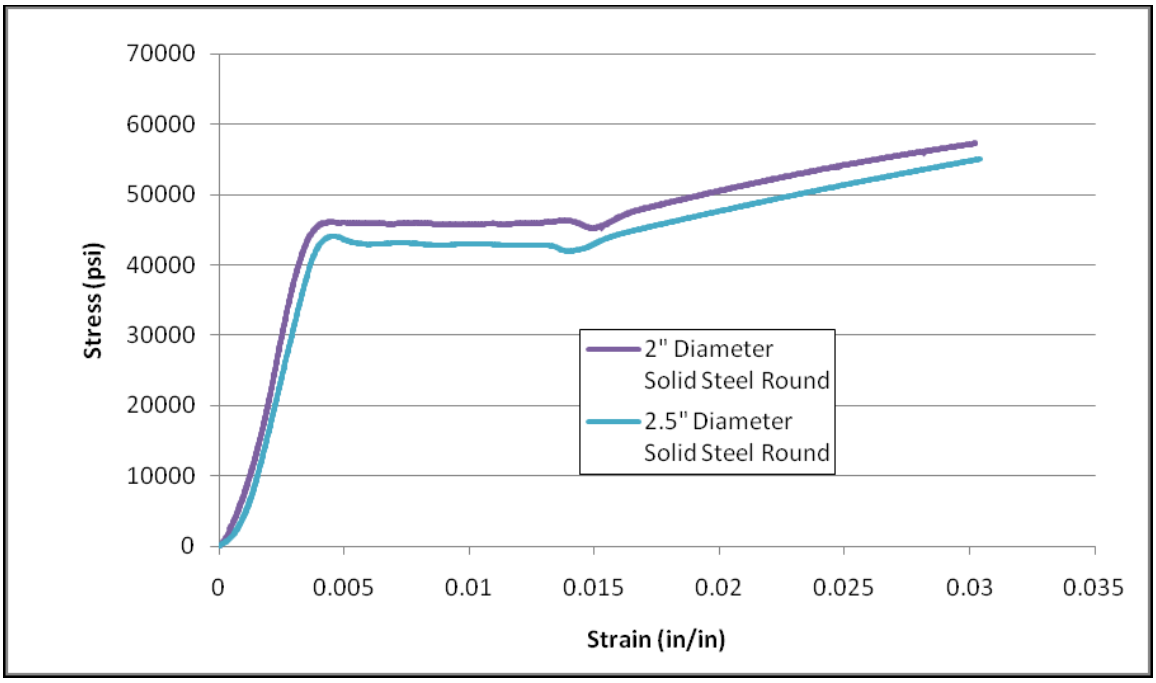

Figure 11: Stress vs. strain for short 12 in. solid steel rounds bars

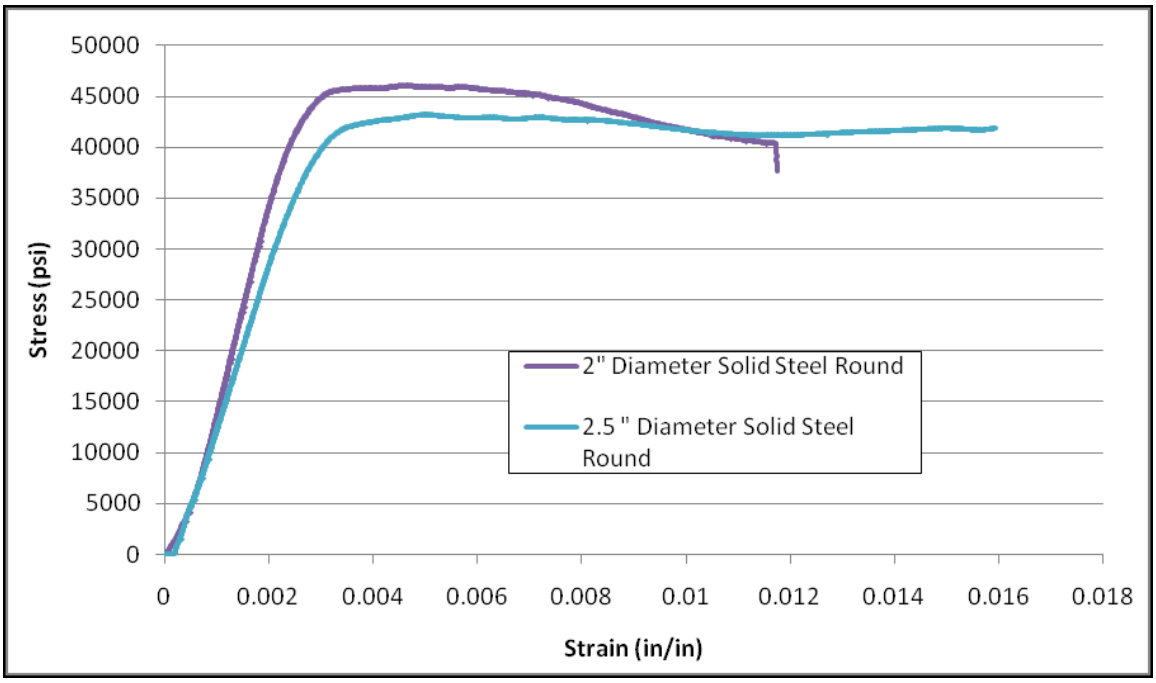

Figure 12: Stress vs. strain for long 24 in. solid steel round bars

big, the biaxial restraint will not be effective because an undesirable amount of deformation from bending of the core will concentrate stress on a relatively small area of the sleeve causing the sleeve to fail prematurely.

A lower boundary can be produced from elastic and inelastic Poisson's ratios of 0.27 and 0.5, respectively. Equations 4, 5 and 6 show the derivation of the increase in diameter of a solid steel round bar in the elastic range.

$$d_n = d + \delta \tag{4}$$

where d_n is the increased diameter due to elastic Poisson's effect, d is the original diameter of the core, and δ is the increase in diameter.

$$\delta = \varepsilon_x * d = \nu * \varepsilon_y * d = \nu * \frac{\sigma_y}{E} * d \tag{5}$$

where ε_x is the strain in the x direction, ε_y is the strain in the y direction, σ_y is the yield stress and E is the modulus of elasticity. Equation 6 is the equation for the increased diameter of a solid round bar under elastic compression and is derived by combining Equations 4 and 5.

$$d_n = d\left(1 + \nu * \frac{\sigma_y}{E}\right) \tag{6}$$

Equations 7 and 8 explain the steps to derive the increase in the diameter for inelastic Poisson's effect for a solid round bar.

$$d_{ni} = d_n + \delta_i \tag{7}$$

where d_{ni} is the increased diameter due to inelastic Poisson's effect, d_n is the increased diameter due to elastic Poisson's effect, and δ_i is the increase in the diameter in the inelastic range. Equation (8) is the increase in the diameter due to inelastic Poisson's effect.

$$d_{ni} = d_n + d_n * \nu_i * \varepsilon_b \tag{8}$$

where υ_i is the inelastic Poisson's ratio, and ε_b is the strain at which the core buckles. Fig. 13 shows the increase in the diameter of the solid round in the elastic and inelastic region.

The lower boundary for the gap distance between the core and the constraining sleeve is found combining Equations 6 and 8 and is represented by Equation 9.

$$lower\ boundary\ gap\ distance = \frac{d\left(\nu + \frac{\sigma_y}{E} + \nu_i * \varepsilon_b + \nu * \nu_i * \frac{\sigma_y}{E} * \varepsilon_b\right)}{2} \qquad (9)$$

Equation 9 is simply the change in diameter of the core from compression. If the core engages the sleeve before the core buckles then the sleeve would not be as effective in constraining the core as it would if the core was allowed to buckle because the sleeve will undertake load at earlier strains causing the system to fail earlier. A lower boundary value for the gap for a 2 in. diameter and 24 in. long solid steel round bar is calculated to be 0.006 in using a compression modulus of elasticity of 32,000,000 psi, a buckling strain of 0.012 in./in. and a yield stress of 46,000 psi. This value is lower than the 0.03 in. gap used for this research.

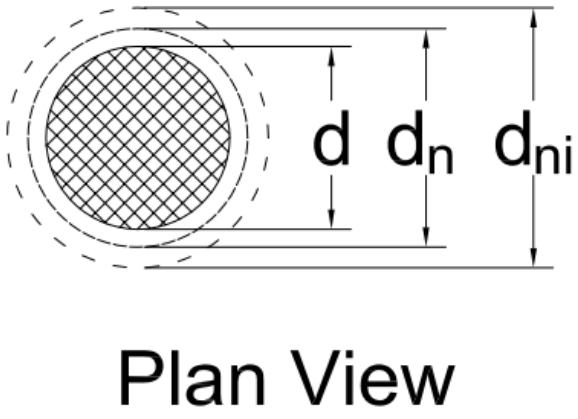

Figure 13: Diameter increase through elastic and inelastic Poisson's effect

Fig. 14 displays how a solid round bar will deflect with hinge-fixed end conditions.

The upper boundary is calculated using Equation 10 for large deflections found in Chajes (1974)

$$\delta = \frac{L * 2 * \sin(0.5\alpha)}{\pi\sqrt{P/P_{cr}}} \tag{10}$$

where δ is the transverse deflection of the core under compressive load as seen in Fig. 14, L is the length of the core, α is the angle made from the hinged end of the core as seen in Fig. 14, P is the experimental buckling load, and P_{cr} is the theoretical buckling load. Table 4 is a summary of the predicted and actual transverse deflections of the compressed solid steel round bars.

Table 4 shows the deflection percent difference to be within 6% and as close as1% percent of the predicted value to the actual measured value. This knowledge gives a

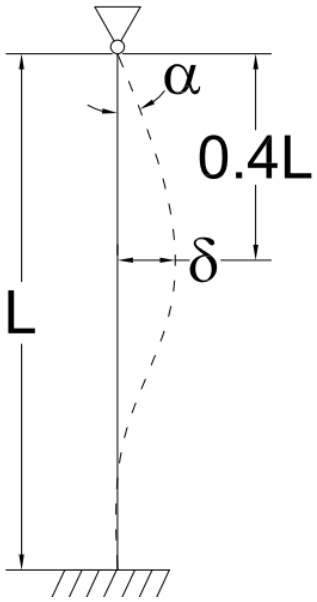

Figure 14: Deformed shape for a compressed bar with hinge-fixed end conditions

Table 4: Predicted and actual transverse deflections

Diameter (in)	Length (in)	α (degrees)	p (radians)	P (lb)	Pcr (lb)	Predicted Deflection (in)	Actual Deflection (in)	Deflection % Difference
2	24	3	0.026	144911	131947	0.38	0.41	6%
2.5	24	3	0.026	215720	208621	0.39	0.41	3%
2	12	3.5	0.031	180275	150796	0.21	0.22	2%
2.5	12	2	0.017	274714	238074	0.12	0.13	1%

good idea how to predict how much transverse deflection the solid steel round bar will experience at the time of buckling. This knowledge in turn can provide an upper boundary of the gap distance.

The point of maximum transverse deflection along the length of the bar can be approximated taking the derivative of Equation 11, an equation found in Chajes (1974)

$$y = \frac{M_0}{P} * \left(\frac{x}{l} + 1.02 \sin\left(4.49 * \frac{x}{l}\right)\right) \tag{11}$$

where M_0 is the moment on the fixed end of the bar, P is the compressive load, x is any point for the length of the bar, and l is the length of the bar. Equation 12 is the derivative, with respect to x, of Equation 6 with the ratio M_0/P set to 1 since they are arbitrary.

$$y' = \frac{4.5798\left(\cos\left(4.49 * \frac{x}{l}\right) + 0.21835\right)}{l} \tag{12}$$

The maximum transverse deflection can be found by setting y' to zero and solving for x. The maximum transverse deflection occurs at a distance of approximately 40% of the length from the hinged end. Fig.14 shows the location of the maximum transverse deflection.

5.5 Short Sleeved Cores

Three 12 in. long specimens were tested two with a lead lining of the gap between the core and the confining sleeve and one without the lead lining. The short specimens are comprised of a 2 in. diameter solid A36 steel core surrounded by a confining sleeve made out of a 2 in. standard seamless pipe. Fig. 15 is a short 12 in. specimen set up for testing in the Instron compression machine.

Fig. 16 is a plot of the stress versus strain of the short specimens tested. S12W1 does not have lead while S12L1 and S12L2 have lead inside the gap. By data reduction, all specimens yielded around 45,000 to 48,000 psi. Yielding in each specimen continued up to 1 percent strain, and then strain hardening began. Specimens S12L1 and S12L2 have a higher stiffness during strain hardening, than S12W1. This is due to the lead lining of specimens S12L1 and S12L2 in that there was effectively a small gap space. Fig. 17 shows the load versus displacement behavior for the short 12 in. sleeved specimen.

Figure 15: Example of short specimen in testing apparatus

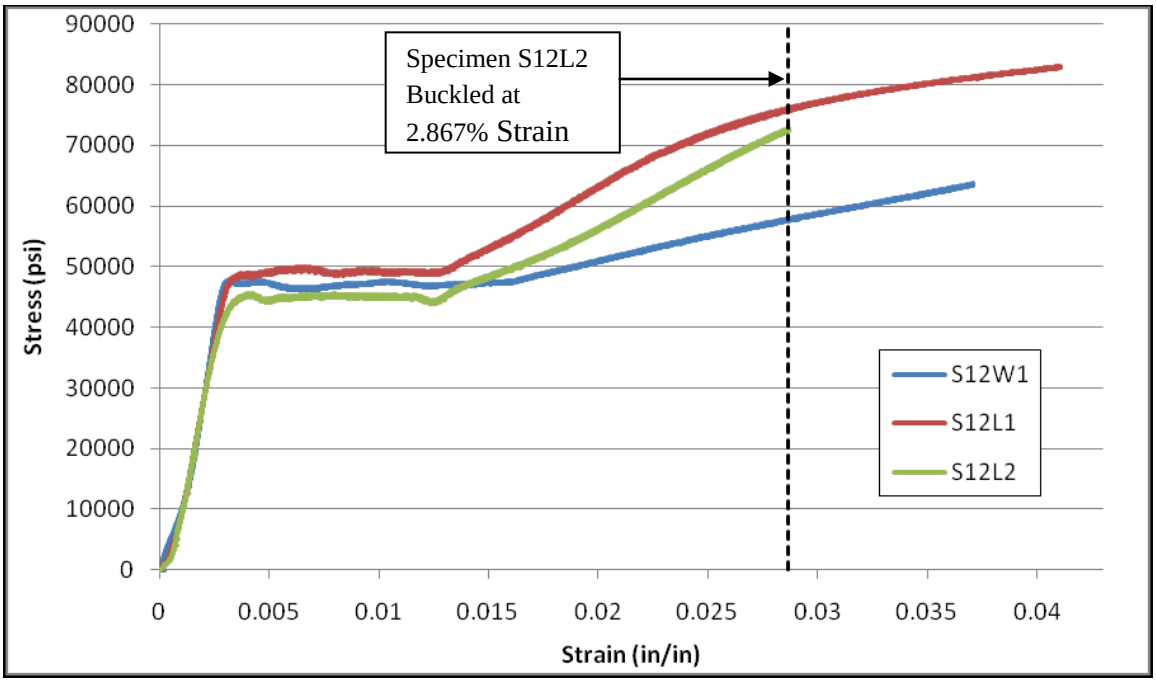

Figure 16: Stress vs. strain for short sleeved 12 in. specimens

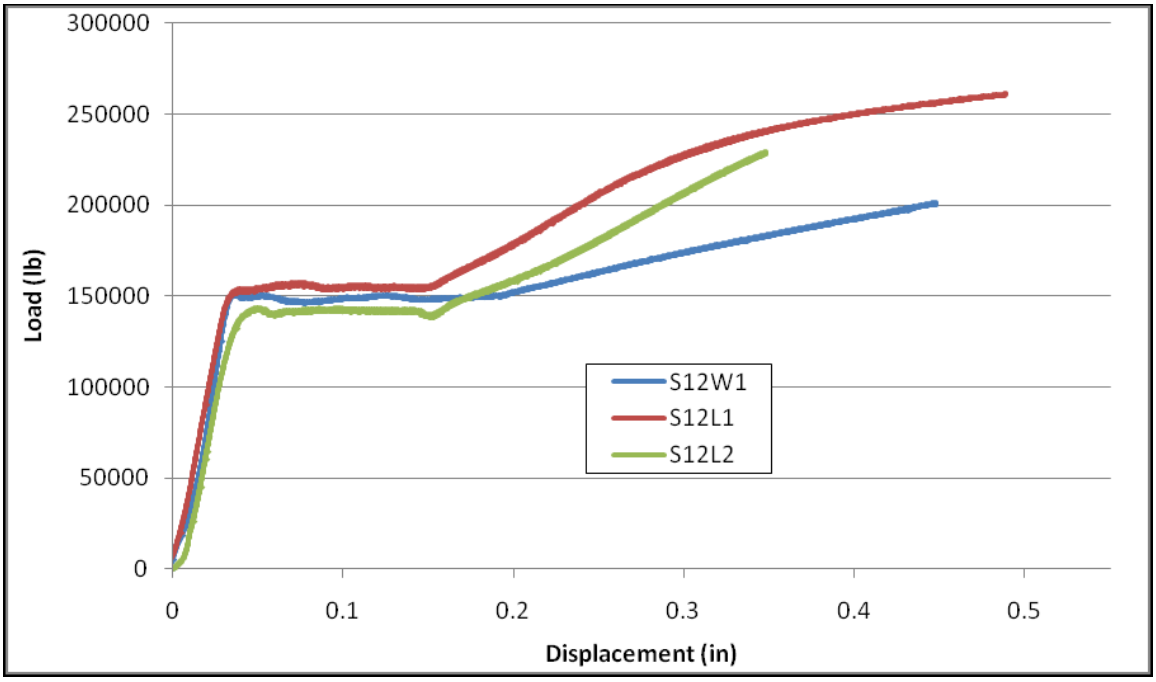

Figure 17: Load vs. displacement for short sleeved 12 in. specimens

Table 5 shows the maximum load and displacement attained in each test. Table 5 also shows the energy dissipated by each specimen. Energy dissipation was determined using Fig. 17, which is a graph of the load vs. displacement for the short 12in. sleeved specimens. Equation 13 is used to calculate the energy dissipated in each specimen in Table 5.

$$E = \int P dL \tag{13}$$

where *P* is the force and *dL* is the change in displacement. Fig. 14 shows the strain at 2.867%, the strain at which specimen S12L2 buckled, of all the short 12 in. sleeved specimens where the calculated energy was determined. Specimens S12L1 and S12L2 dissipated more energy at a 2.867% strain than specimen S12W1. The lead in the gap of S12L1 and S12L2 enabled the core to engage the sleeve earlier than S12W1 which has no lead and a larger gap. S12L1 dissipated considerably more energy than S12L2. It is also observed that the specimens with lead dissipate energy earlier than the specimen without lead.

Testing for two of the three short specimens was stopped before failure could take place. Specimen S12L1 visually buckled and the testing was terminated even though the load was still increasing.

Table 5: Energy dissipation, maximum load, maximum stress, and maximum displacement for short sleeved specimens

Type	Test	Max Position (in)	Max Load (lb)	Max Stress (psi)	Energy Dissipation @ 2.867% Strain (kip-in)	Percent Strain Energy Gained (%) Based on S12W1
No Lead	S12W1	0.547	226686	71654	43.5	0%
Lead	S12L1	0.501	261728	83061	59.3	15%
Lead	S12L2	0.348	229212	72597	54.2	5%

Strain gauge data were collected. Strain gauge data were used to determine three aspects of behavior observed in the tests: (1) when the core expanded enough to engage the sleeve; (2) when the sleeve steel yields; and (3) if there is axial load in the constraining sleeve. Strain gauges were positioned to detect radial strain on the sleeve in locations approximately 1 in. from the top and bottom and at the middle of the core. A strain gauge was placed on the constraining sleeve to detect axial strain and positioned to represent the middle of the core as shown in Fig. 2.

Strain gauge activity for each specimen is unique because of the characteristics of each specimen. Strain gauges show negative and positive data; this is due to induced bending in the outer sleeve. The bending is due to an uneven radial expansion of the steel cores.

The strain gauge data for specimen S12W1 are shown in Fig. 18. It is observed from Fig. 18 that the core engages the sleeve when the stress in the core reaches 47,500 psi. At higher stresses the top and bottom strain gauges show an increase in activity while the middle strain gauge shows little activity. It is assumed the core yielded at the top and bottom causing the sleeve to acquire axial load. The increase of axial strain at mid-height can also be observed in Fig. 18. Fig. 19 and Fig. 20 show an elevation and top view of the specimen after the compression test, respectively. Testing for S12W1 was terminated before buckling failure could occur.

Strain gauge data collected for S12L1 in Fig. 21 suggest buckling occurred toward the top of the specimen. The core engaged the constraining sleeved at a stress of 48,000 psi. The top strain gauge yields at lower stresses than the middle, bottom and axial strain gauges. The axial and middle strain gauges begin yielding when the core is

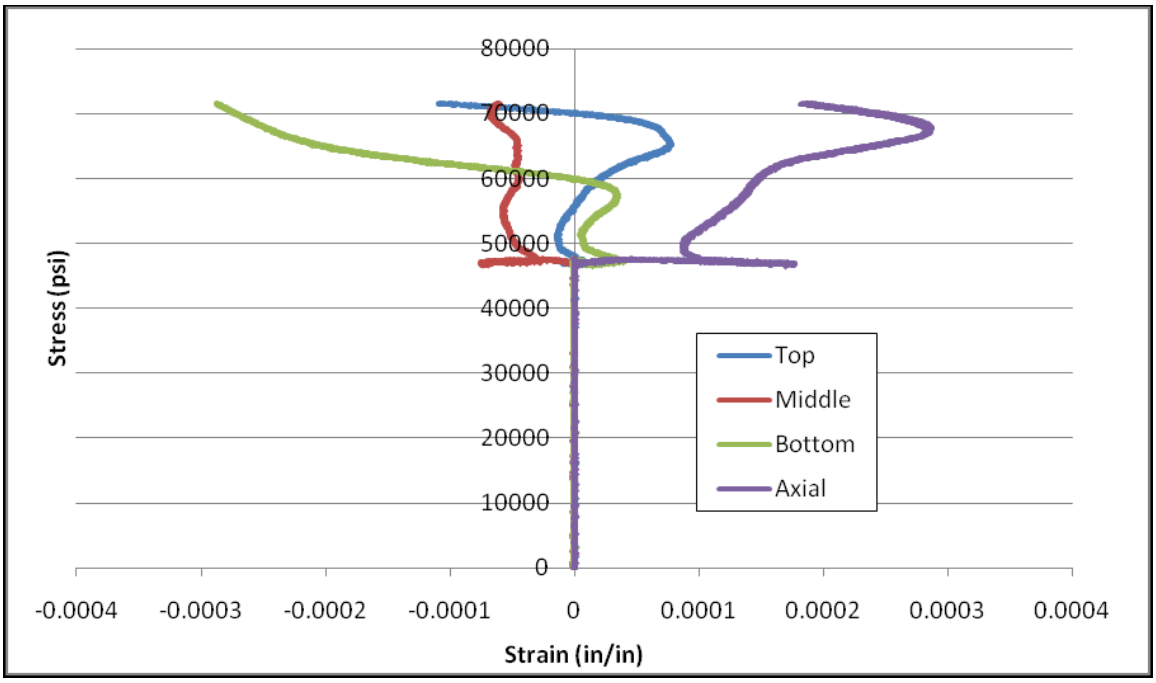

Figure 18: Strain gauge data for S12W1

Figure 20: Elevation view of specimen S12W1

Figure 19: Top view of specimen S12W1

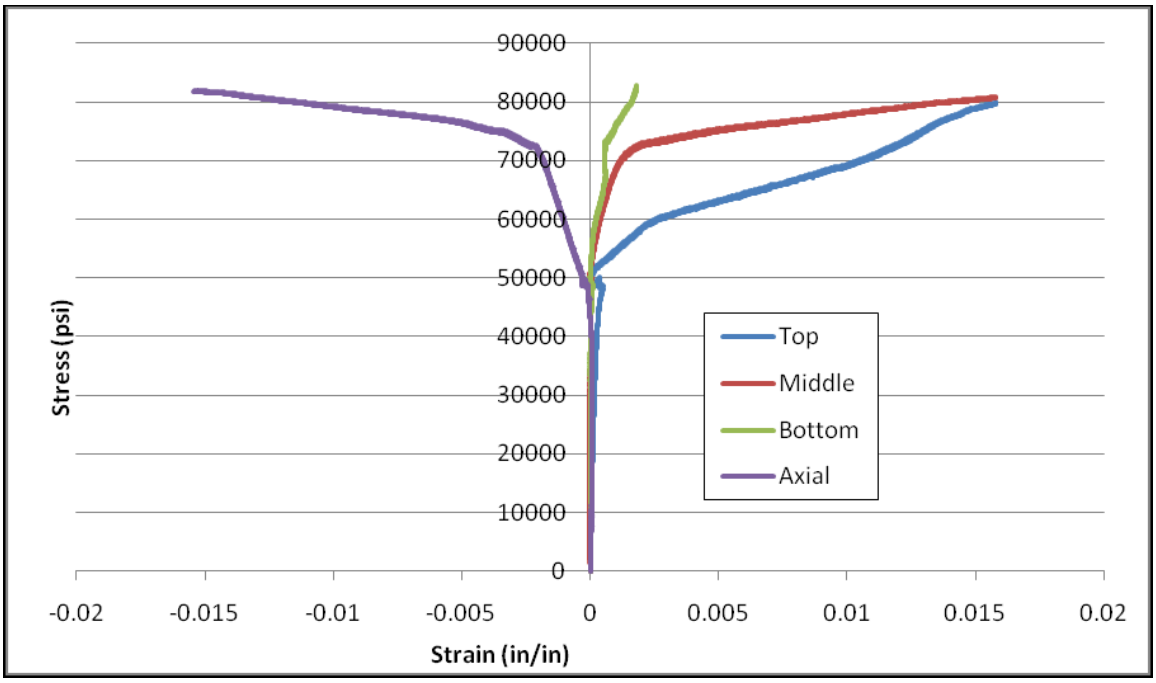

Figure 21: Strain gauge data for S12L1

compressed approximately 72,000 psi and the strain of the bottom strain gauge increases only slightly. Fig. 22 shows the specimen after the compression test. This specimen buckled. Stress lines were developed on the constraining sleeve, indicating the specimen did buckle towards the top of the specimen. Fig. 23 shows the top of the specimen. The 1 in. high strength steel plug used in the testing apparatus was pinched in the constraining sleeve.

Strain gauge data for specimen S12L2 are shown in Fig. 24. The core engaged the constraining sleeve at a stress of 45,000 psi. The top strain gauge shows most of the strain activity after the core engaged the sleeve. This suggests yielding occurred at the top of the specimen. Axial strain gauge data show the constraining sleeve did obtain axial load. Fig. 25 and Fig. 26 show the elevation and top view of specimen S12L2, respectively. It can be seen in Fig. 25 that the specimen buckled.

Figure 22: Elevation view of specimen S12L1

Figure 23: Top view of specimen S12L1

Testing for the short specimens determined the compressive strength of the core, the energy dissipation, and how the specimens failed. The short 12 in. specimens were not compressed to large buckled shape therefore long specimens were prepared and tested.

The gauges applied to the sleeve in a radial manner experienced tension and compression. Intuitively the radial strain gauges should only show tension because of the expansion of the sleeve from the Poisson's effect of the core. Fig.27 is a diagram explaining the mechanics and deformed shape of the sleeved specimens under a compressive load. The arrows at Location 1 represent the force acting on the sleeve from the expansion of the core under compressive load. Through testing of the solid steel round bars expansion began and remained predominantly in the top and bottom portions

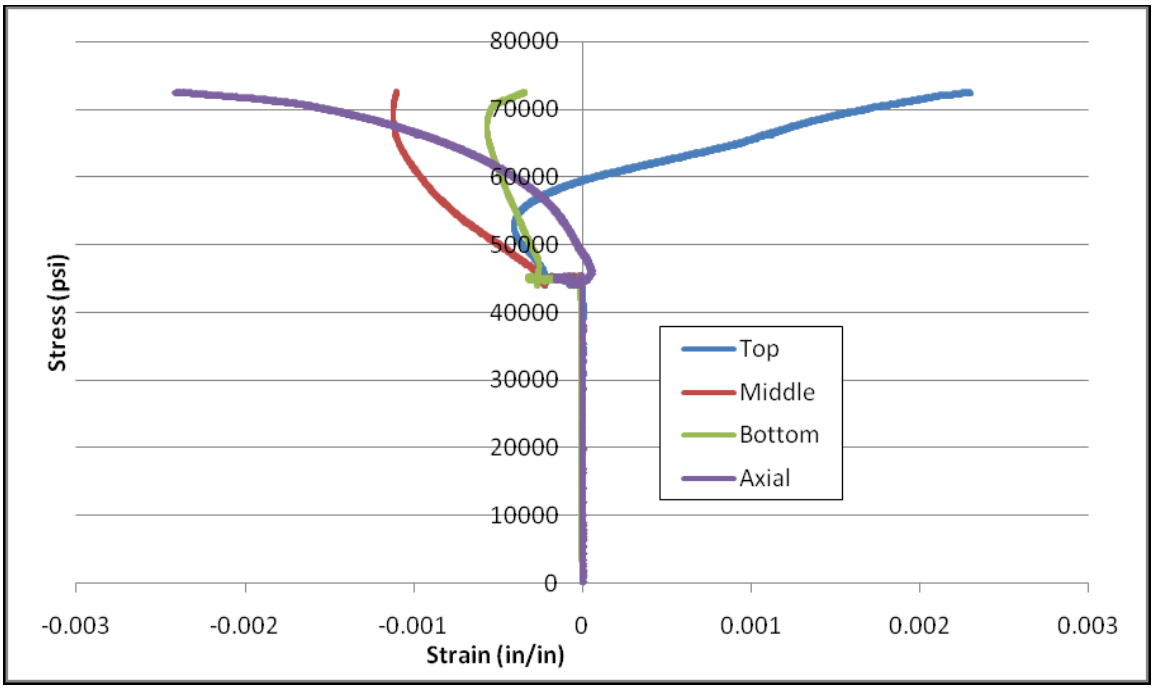

Figure 24: Strain gauge data for S12L2

Figure 25: Elevation view of specimen S12L2

Figure 26: Top view of specimen S12L2

of the bars through compression until the bars buckled. Because the top of the bars expanded, the sleeve expanded on the top, forcing a curved shape sleeve pipe. As the sleeve is pushed out at Location 1 the sleeve at Location 2 pushes in towards the core. The small arrows at Location 2 represent a smaller magnitude of force than that of Location 1 as the sleeve engages the core and the core pushes back.

The deformed shape described in Fig. 27 represents the top of the specimen as well as the bottom of the specimen. The explanation of the mechanics of the sleeved specimen under compressive load also explains why the strain gauges recorded readings of tension and compression.

5.6 Long Sleeved Specimens

Three 24 in. long specimens were tested: two with lead lining the gap between the core and the confining sleeve, and one without the lead lining. Fig. 28 is a picture of a

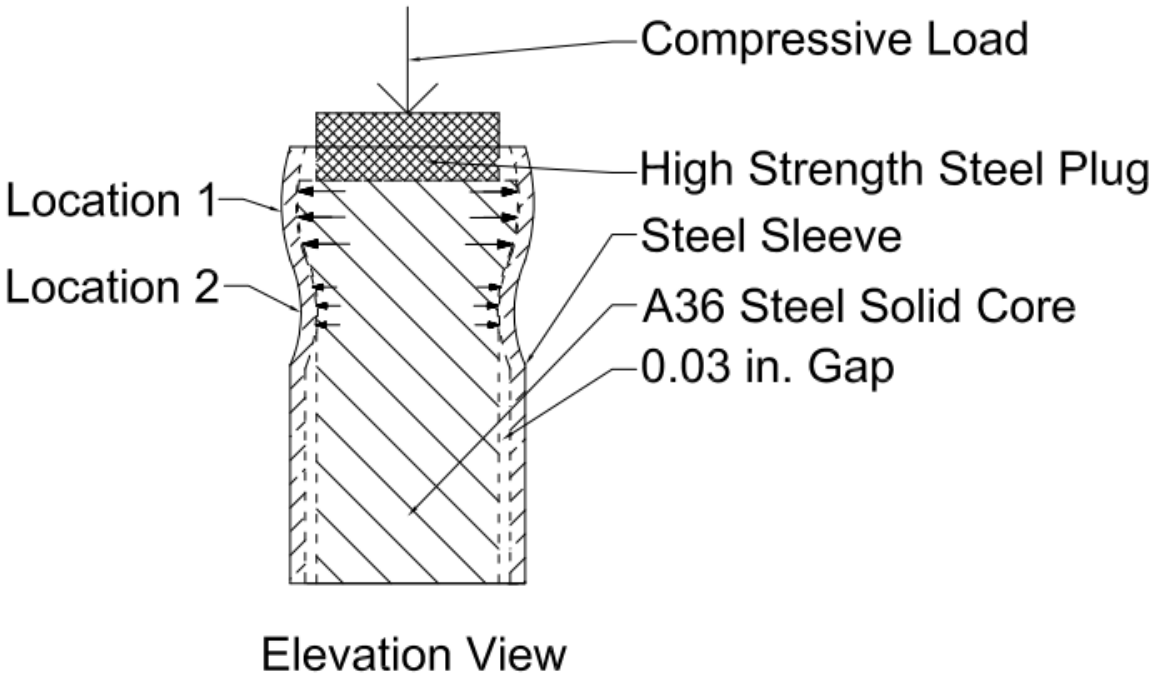

Figure 27: Schematic of deformed shape of specimen

Figure 28: Example of long specimen in testing apparatus

long specimen in the Instron compression machine. The long specimens are comprised of a 2 in. diameter solid A36 steel core surrounded by a confining sleeve made out of a 2 in. standard seamless pipe.

Fig. 29 is a plot of the stress versus strain of the long specimens. L24W1 does not have lead while L24L1 and L24L2 have lead inside the gap. By observation all specimens yielded around 45000 to 49000 psi. Soon after initial yielding of the core both specimens with lead began to strain harden. The specimen without any lead yielded longer than the other two specimens. This is due to the lead in the gap enabling the core to engage the constraining sleeve at earlier strains. Fig. 30 shows the load versus displacement behavior of the long 24 in. sleeved specimens.

Table 6 shows the maximum load and displacement of the long specimens. Table 6 also shows the energy dissipation at 2.5% strain. Energy dissipation was determined using Fig. 28. Energy is determined using Equation 13. For the long specimens with lead

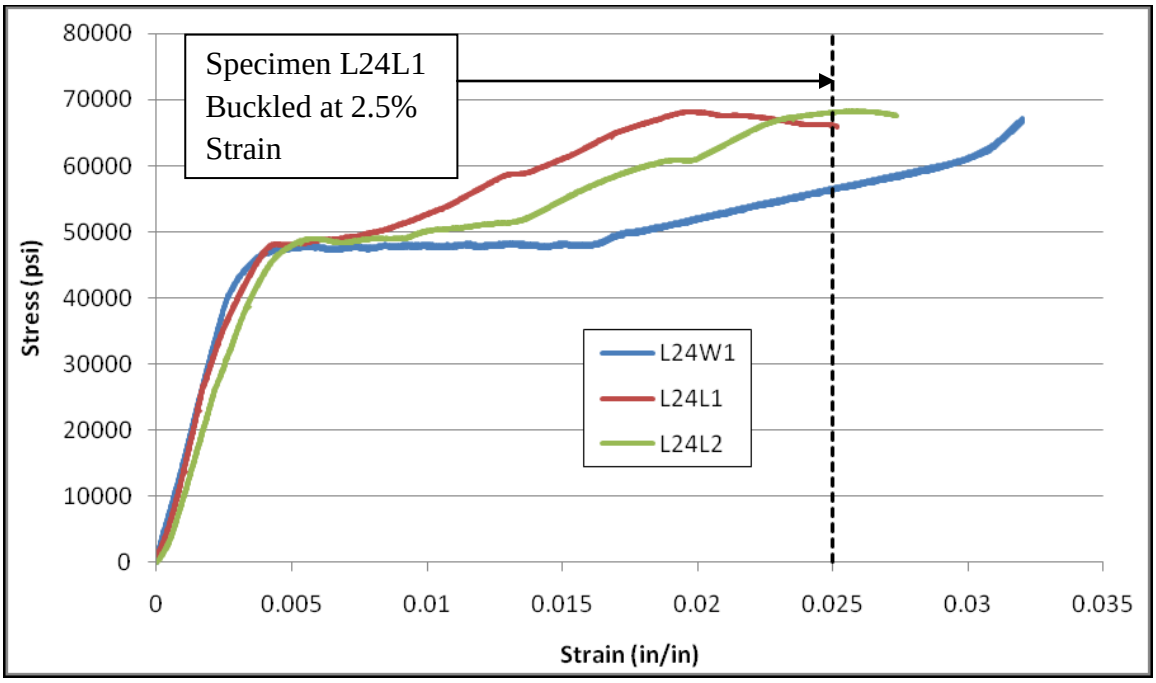

Figure 29: Stress vs. strain for long 24 in. sleeved specimen

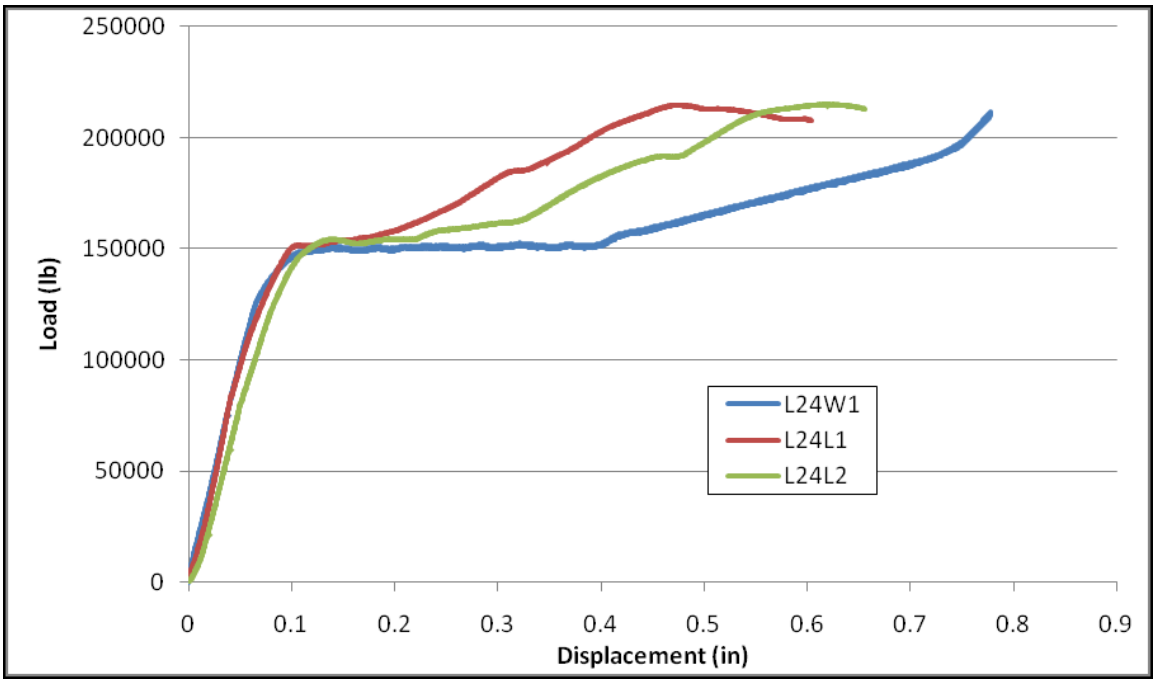

Figure 30: Load vs. displacement for long 24 in. sleeved specimen

Table 6: Energy dissipation, maximum load, maximum stress and maximum displacement for long sleeved specimens

Type	Test	Max Position (in)	Max Load (lb)	Max Stress (psi)	Energy Dissipation @ 2.5% Strain (kip-in)	Percent Strain Energy Gained (%) Based on L24W1
No Lead	L24W1	0.778	211656	67037	87.4	0%
Lead	L24L1	0.579	214715	68073	95.3	9%
Lead	L24L2	0.635	213968	67972	95.4	9%

the percent gain of energy dissipation is approximately 9% greater than without lead. The specimens with lead dissipate energy faster at lower strains than the specimen without lead. This trend is similar to the behavior of the short sleeved specimens. It is clear that as the length increases, a proportionally larger amount of energy is dissipated.

Specimens L24L1 and L24L2 failed in buckling during the compression test. Specimen L24W1 did not fail in compression; the test was terminated once the constraining sleeve engaged the top plate of the testing apparatus inducing axial load on the constraining sleeve.

Strain gauges were attached to the constraining sleeve of the long specimens in the same manner as for the short specimens. They were attached to the constraining sleeve approximately 1 in. from the top and bottom of the specimen and at the middle of the specimen.

Strain gauge data were collected for specimen L24W1. The core engaged the constraining sleeve at approximately 48,000 psi. Fig. 31 is a plot of the stress of the core and the strain in the constraining sleeve at various locations. This plot shows the top, middle, and bottom strain gauges with similar strain activity after the core engages the

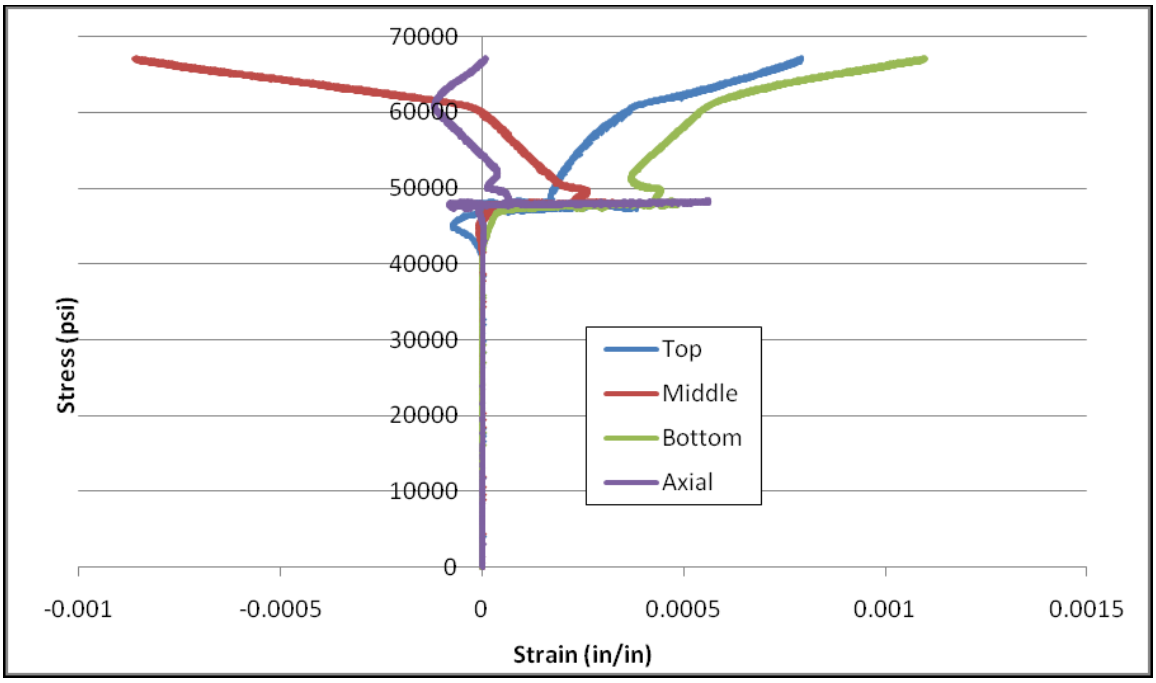

Figure 31: Strain gauge data for L24W1

sleeve. The axial strain gauge shows little strain activity, indicating the core was not binding in this test and the sleeve did not experience a great deal of load. This is due to the larger gap between the core and the constraining sleeve. This test terminated early because the top plate of the testing apparatus engaged the constraining sleeve; the specimen did not visually buckle.

Figs. 32 and Fig. 33 show an elevation and top view of the specimen after the compression test, respectively.

Strain gauge data were collected for specimen L24L1. The core engaged the constraining sleeve at approximately 48,000 psi. Fig. 34 is a plot of the stress of the core and the strain in the constraining sleeve at various locations. The top and axial strain gauges show early stain activity once the core engaged the constraining sleeve. The bottom and middle strain gauges showed little strain activity until buckling of the specimen had occurred. After the specimen buckled, the bottom strain gauge increased in

Figure 32: Elevation view of specimen L24W1

Figure 33: Top view of specimen L24W1

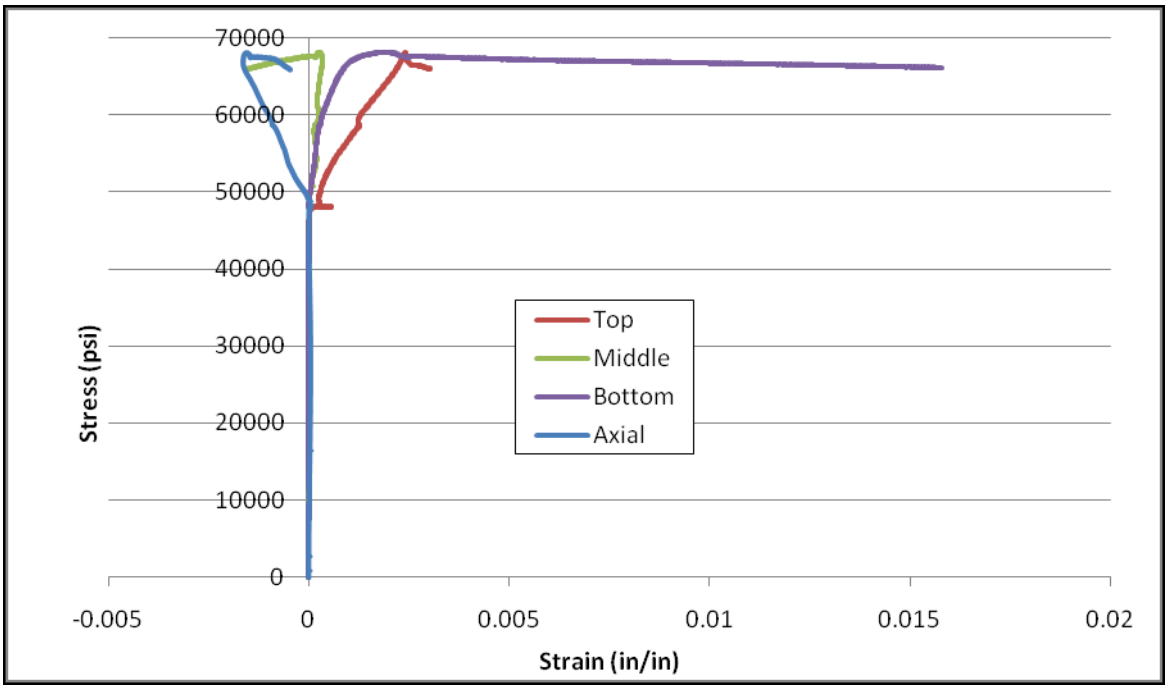

Figure 34: Strain gauge data for L24L1

radial strain dramatically, indicating that buckling had occurred towards the bottom of the specimen. Fig. 35 visually shows where the specimen buckled. Fig. 36 is a top view of L24L1.

Strain gauge data for Specimen L24L2 was collected. According to Fig. 37 the core was in contact with the constraining sleeve from the beginning of the test. The axial strain gauge shows load being transferred into the sleeve at early core stresses. Fig. 37 shows the core engaging the constraining sleeve at approximately 48,500 psi. After the core engaged the constraining sleeve all radial strain gauges show a large amount of strain activity. After specimen L24L2 buckled all strain gauges show increased amounts of strain activity. The axial strain gauge indicates that the specimen underwent axial compression loading and then tension before failure. Fig. 38 and Fig. 39 show elevation and top view of specimen L24L2; buckling has clearly occurred.

Figure 35: Elevation view of specimen L24L1

Figure 36: Top view of specimen L24L1

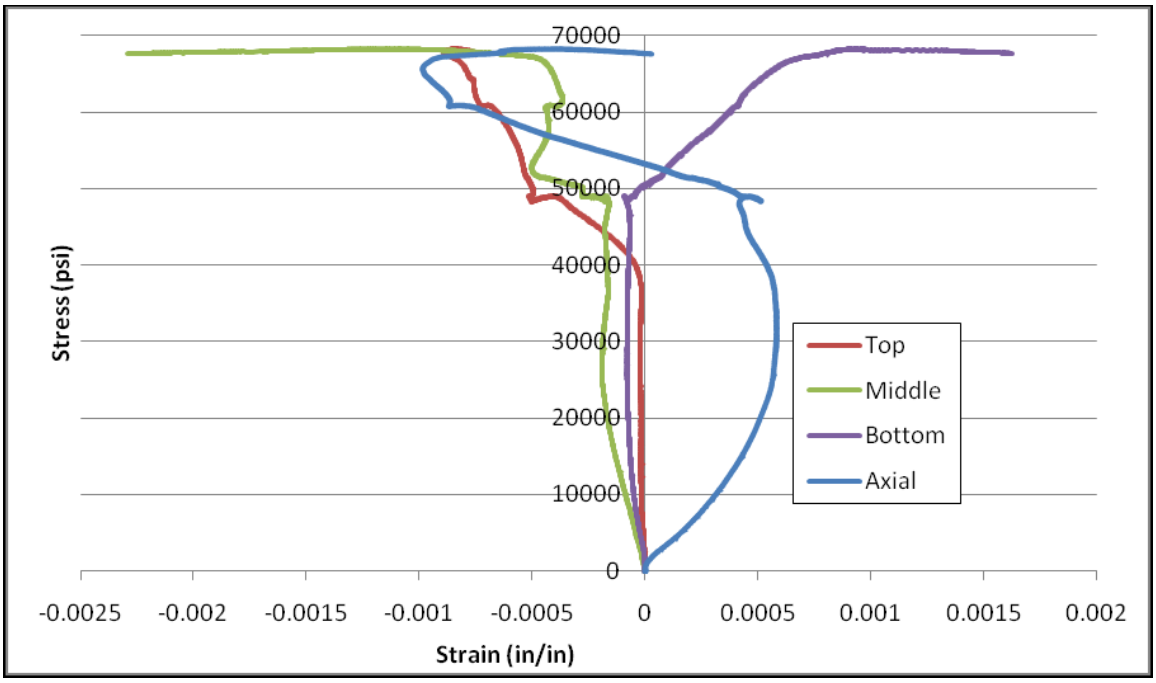

Figure 37: Strain gauge data for L24l2

Figure 38: Elevation view of specimen L24L2

Figure 39: Top view of specimen L24L2

An interesting detail of specimens L24L1 and L24L2 is a second plateau of the stress to the core before ultimate failure. This yield takes place at approximately 58,500 and 60,600 psi for specimens L24L1 and L24L2, respectively. This yielding can also be seen in Fig. 29. A corresponding abrupt change in the strain can be seen in the strain gauge data (Fig. 34 and Fig. 37) at approximately the same stress in each specimen. This abrupt change is due to the inner core buckling.

Fig. 27 is an explanation of how the core interacts with the sleeve and an explanation of how the radially placed strain gauges on the core gave readings of compression and tension. The long sleeved specimen reacted in the same manner as the short sleeved specimen

6. DISCUSSION

6.1 Introduction

This section discusses the differences between the solid steel round bars and the sleeved compression members dealing with energy dissipation and the slenderness of each specimen.

6.2 Energy Dissipation

Figs. 40 and 41 are plots of the stress versus strain of the solid steel round bars and the sleeved compression members short and long respectively. These figures show the differences between the sleeved compression members and the solid steel round bars. For both the long and short specimens the sleeved compression members failed at higher stresses and strains. It is interesting to note that the 2.5 in. diameter solid steel round bars, fail at smaller stresses and strains than all three of the compression sleeved members. This compares well to the 2.38 in. outer diameter of the pipe because this shows that the sleeved compression member is not acting as one member, but as two components: a compression core and a sleeve to resist bending in the core.

Tables 7 and 8 show the maximum displacement, maximum load, total energy dissipation and percent of strain energy gained for all specimens at the time the test was terminated. Table 7 shows that the short 2.5 in. solid steel round bar could resist the most force, due to a larger cross-sectional area, but in energy dissipation it was the lowest

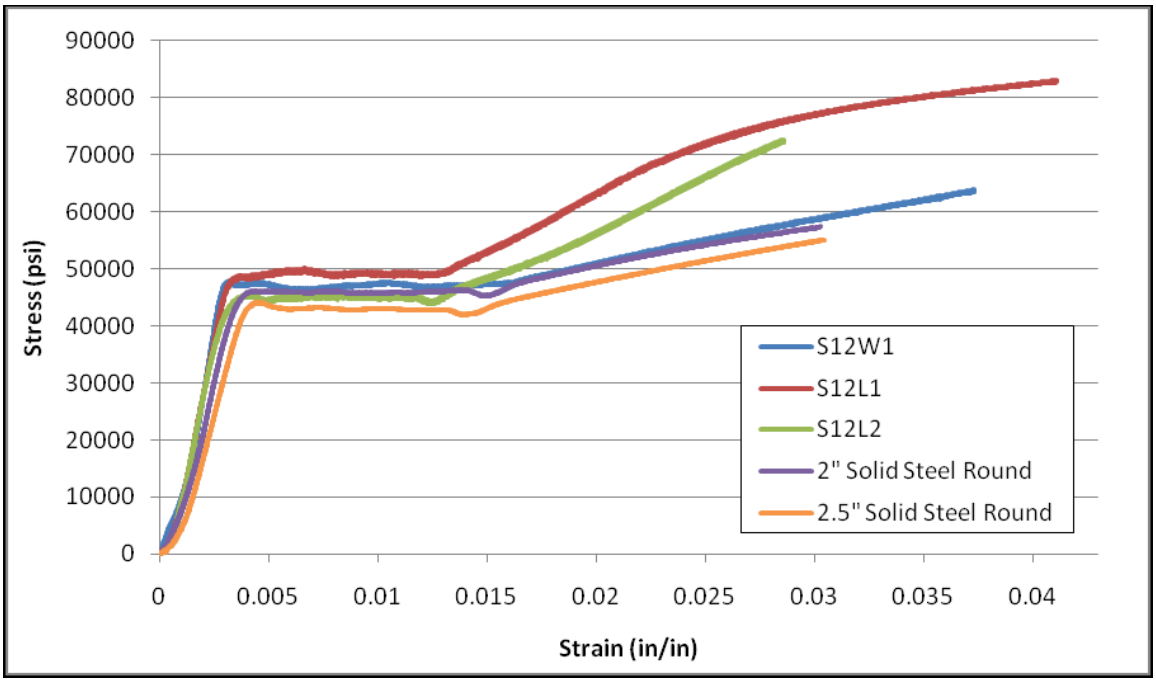

Figure 40: Stress vs. strain for all short specimens

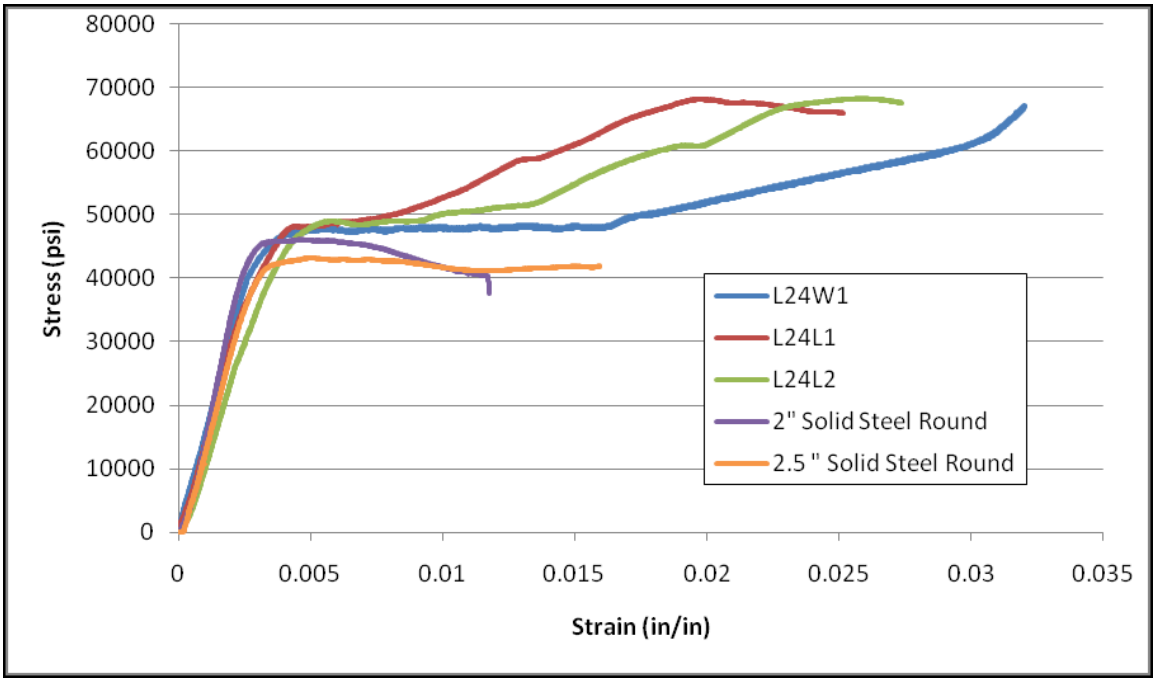

Figure 41: Stress vs. strain for all long specimens

Table 7: Energy dissipation, maximum load, maximum stress and maximum displacement for all short specimens

Type	Test	Max Position (in)	Max Load (lb)	Max Stress (psi)	Percent Max Load Gained (%)	Total Energy Dissipation @ Termination (kip-in)	Percent Strain Energy Gained (%) Based on 2 in. Diameter
2" Diameter	12in	0.302	180275	57383	0%	52.4	0%
2.5" Diameter	12in	0.369	274714	55964	52%	79.3	51%
No Lead	S12W1	0.547	226686	71654	26%	88.3	68%
Lead	S12L1	0.501	261728	83061	45%	97.4	86%
Lead	S12L2	0.348	229212	72597	27%	54.2	3%

Table 8: Energy dissipation, maximum load, maximum stress and maximum displacement for all long specimens

Type	Test	Max Position (in)	Max Load (lb)	Max Stress (psi)	Percent Max Load Gained (%)	Total Energy Dissipation @ Termination (kip-in)	Percent Strain Energy Gained (%) Based on 2 in. Diameter
" Diameter	24in	0.282	144911	57383	0%	34.3	0%
2.5" Diameter	24in	0.382	215720	55964	49%	72.3	110%
No Lead	L24W1	0.778	211656	71654	46%	119.2	247%
Lead	L24L1	0.579	214715	83061	48%	96.1	180%
Lead	L24L2	0.635	213968	72597	48%	107.4	212%

percent gain over the short 2 in. solid steel round bar other than specimen S12L2. Table 8 shows the same trend, but the percentage difference between the long 2.5 in. solid steel round bar and the long sleeved compression members is greater than in the short specimens. It is interesting to note that in this study the energy dissipated doubles as the length doubles from 12 in. to 24 in.

6.3 Slenderness

Slenderness is an issue that needs to be considered. Slenderness is defined by *kl/r* where *k*, the effective length factor, accounts for the end conditions, *l* is the length and *r* is the radius of gyration. Depending on the slenderness and material, a designer can determine when a material will fail under axial load and whether failure will occur in the elastic or inelastic range. The specimen lengths used in this research are rather short and all specimens failed in the inelastic region.

Table 9 shows the *kl/r* or slenderness values calculated for the steel core of each specimen. Fig. 42 shows a plot of load versus slenderness. The points in Fig. 42 correspond to the points given in Table 8. The plot shows the decrease in load as the slenderness increases. Though the steel core of each of the sleeved compression members has the same slenderness as the 2 in. diameter solid steel round bars, the values for load are closer to the 2.5 in. diameter solid steel round bars showing the increase in load of the sleeved compression members.

Fig. 43 is a plot of the energy versus slenderness. This plot shows that the dissipated energy for the solid steel round bars will decrease as the slenderness increases, but the sleeved compression members dissipate more energy as the slenderness increases. It is assumed that the increase in energy dissipation will only increase until the

Table 9: Slenderness of steel core sleeved specimens

Type	Test	Length (in)	Diameter (in)	kl/r	Max Load (lb)	Total Energy Dissipated (kip-in)
2.5" Diameter	12in	12	2.5	13.44	274714	79.3
2" Diameter	12in	12	2	16.8	180275	52.4
No Lead	S12W1	12	2	16.8	226686	88.3
Lead	S12L1	12	2	16.8	261728	97.4
Lead	S12L2	12	2	16.8	229212	54.2
2.5" Diameter	24in	24	2.5	26.88	215720	72.3
2" Diameter	24in	24	2	33.6	144911	34.4
No Lead	L24W1	24	2	33.6	211656	119.2
Lead	L24L1	24	2	33.6	214715	96.1
Lead	L24L2	24	2	33.6	213968	107.4

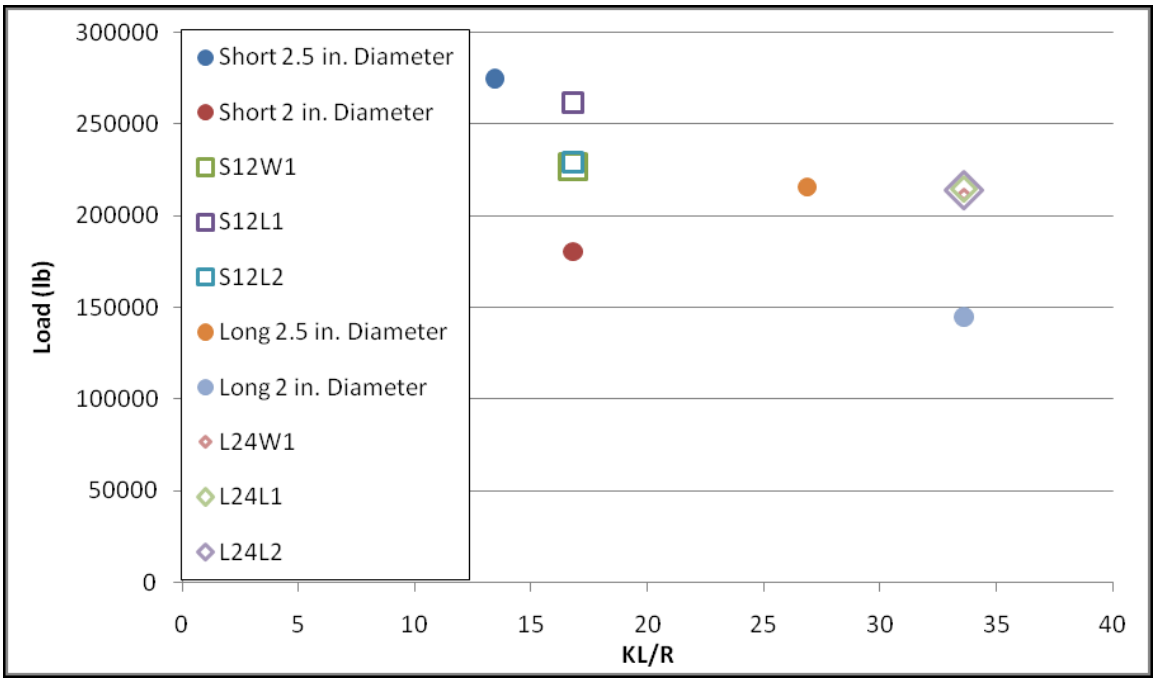

Figure 42: Load vs. slenderness

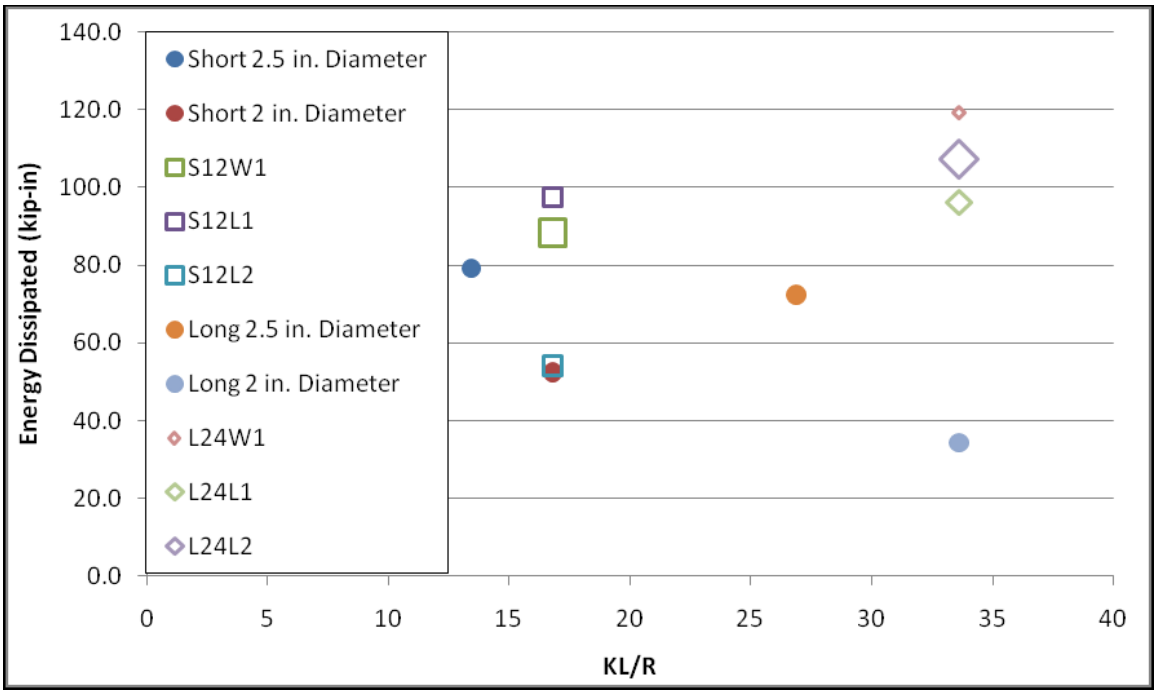

Figure 43: Energy dissipated vs. slenderness

slenderness is in the elastic range. An optimization of this characteristic will have to be studied further through testing.

Specimens with larger slenderness will need to be tested further to gain a better understanding of the characteristics of the specimens in the elastic range.

7. CLOSURE

7.1 Conclusions

This study concerns the behavior of steel sleeved compression members with steel cores at two different lengths. The study also includes the compression of four solid steel round bars of two diameters with two different lengths. Compression tests were performed on all specimens to determine the increase in compressive strength of a steel core element with a buckling restraining steel sleeve and the effectiveness of lead as an intermediate material.

It is concluded that:

- The sleeved compression members did increase in compressive strength compared to unsleeved specimen
- The sleeved compression members did increase in energy dissipation compared to the unsleeved specimen
- The lead was an appropriate intermediate material

In the short specimens an increase of up to 45% in compressive strength compared to a core without a restraining sleeve and a 48% increase for the long specimens were observed.

The 2.5 in. diameter solid steel round bars show slightly greater compressive strength (1% to 8%) before failure compared to the 2.0 in. diameter sleeved compression member specimens, but the 2.5 in. diameter solid steel round bars did not dissipate

energy as well as sleeved compression member specimens. Energy dissipation did increase with the sleeved compression members. Energy dissipation for short sleeved compression members gained up to an 85% increase whereas the 2.5 in. diameter solid steel round bar gained approximately 51%. The long sleeved compression members gained substantially more energy dissipation with an increase of up to 246%, while the 2.5 in. diameter solid steel round bar gained only 110%. More testing will need to be conducted in order to provide an optimization of compressive strength and energy dissipation of sleeved compression members.

The lead was an appropriate material as it did reduce the friction between the solid steel core and the steel sleeve. Additional research should be considered to determine the proper gap distance between the core and the sleeve to fully develop the lead for friction reduction. The specimens with the gap, but without the lead achieved greater strains of the inner core before engaging the outer sleeve. The specimens with the lead intermediate material engaged the outer sleeve at earlier strains right after yielding of the core. When the core begins engaging the sleeve, the energy dissipation of the system begins increasing. It is recommended to use the intermediate material when early energy dissipation is required for design purposes. For applications where energy dissipation is not required until a significant yielding plateau of the steel core has occurred, it is recommended that a gap be left without any intermediate material.

7.2 Future Considerations

Two considerations for further research include exploration into different materials for the intermediate material and industry applications of the biaxially restrained loaded steel cores.

This study used an intermediate material to separate the inner core from the outer sleeve of the sleeved compression member and to reduce the friction between the two components during the compression of the core. During testing this intermediate material is sandwiched between the inner core and the outer sleeve and sheared as the inner core and the outer sleeve slide with respect to each other. Lead was selected as the intermediate material because of the softness of the material allowing it to compress and shear without losing the original properties of the material.

Other materials could be used for the same purpose, including Mylar, polyurethane, graphite foil, or sapphire sheets. Each of these materials has characteristics that could improve the performance of the sleeved compression members. Mylar is a polyester film developed for high tensile strength and has the ability to perform under extreme climates. Mylar can reduce the friction between the inner core and the outer sleeve of the sleeved compression member. Polyurethane is a polymer; its application is suggested because of its use in rubber bushing isolators in vehicle suspension. As a rubber bushing it separates the metal and allows for movement in a similar manner as needed for an intermediate material in a sleeved compression member. Graphite foil has desirable characteristics for sleeved compression members; these characteristics include the ability to perform under extreme high and low temperatures, resist friction by self-lubricating, and corrosion resistant properties. Graphite foil is a good choice for the sleeved compression members. Sapphire is one of the hardest materials in the world and has an astounding low coefficient of friction; the low coefficient of friction is achieved by the breaking down of the sapphire crystals. Manufacturers of sapphire sheets can grow the crystals in all shapes including curved shapes.

These are a few examples of materials that might be suitable for an intermediate material within a sleeved compression member. They all hold unique characteristics that could improve the performance of the sleeved compression members studied in this thesis.

The sleeved compression member can benefit the industry in several applications. These applications include controlled rocking frames, buckling restrained braces (BRB), and vehicle bumper technology.

Controlled rocking frames are being developed by several researchers (Eatherton et al. 2008; Eatherton et al. 2010; and Ma et al. 2010). The idea for the controlled rocking frame is to use prestressing strands to anchor the center of a building to the ground while allowing the frame of the structure to rock. The rocking action requires the base of the building to lift up from the ground and then rock back. After seismic activity, in theory, the building should move back to its original position because of the prestressing strands holding the building in place. This type of technology can reduce structural damage to buildings. Because the frame rocks and lifts up and then slams into the ground, axial members used in the controlled rocking frame undergo a beating. The use of sleeved compression members in all compression members will increase the energy dissipation and life of the frame.

BRB technology can benefit greatly from steel sleeved compression members. Currently BRB's consist of a yielding core surrounded by a concrete filled hollow structural section. The concrete and the yielding core are separated by a material that will not allow the concrete to bond to the core. This unbonding of the core and concrete allows the core to move freely during the yielding process. Manufacturing of this type of

BRB is expensive and time consuming because the BRB has to be lifted in the vertical position on end for the casting of concrete; in addition concrete takes days to cure. The sleeved compression members are made of a steel core and a steel sleeve. Achieving the same energy dissipation performance from the sleeved compression member as that of a traditional BRB will increase productivity because it will reduce manufacturing time.

Bumpers on vehicles could benefit from the sleeved compression member found in this thesis. Bumpers require high early energy dissipation to be able to stop a moving vehicle. Studies on bumper technology have been written about the use of several axial yielding members with steel sleeves restraining the buckling of the member. The use of an intermediate material as found in the sleeved compression members in this study can improve the performance of the bumpers by decreasing the probability that members will bind early by reducing the friction between the core and the sleeve.

In conclusion, the tests conducted on the sleeved compression members were a success and observations and recommendations were given. It is recommended that more testing and analysis be conducted to gain a better understanding of the sleeved compression members and the behavior and characteristics attributed to them.

REFERENCE

American Institute of Steel Construction. (1993). *Load and Resistance Factor Design Specifications for Structural Steel Buildings.* Chicago, Illinois.

American Institute of Steel Construction. (2006). *Steel Construction Manual.* Chicago, Illinois.

American Society for Testing Materials. (2008). *A106/A106M-08 Standard Specification for Seamless Carbon Steel Pipe for High-Temperature Service.*

American Society for Testing Materials. (2008). *A36/A36M-08 Standard Specification for Carbon Structural Steel.*

Beer, F. P., Johnson, E. R., & DeWolf, J. T. (2006). *Mechanics of Materials* (4th ed.). New York: McGraw-Hill.

Chajes, A. (1974). *Principles of Structural Stability Theory.* Englewood Cliffs, New Jersey: Prentice-Hall, Inc.

Construction, A. I. (2006). Steel Construction Manual. Chicago, Illinois.

Eatherton, M. R., Hajjar, J. F., Deierlein, G., Krawinkler, H., Billington, S., & Ma, X. (2008). Controlled Rocking of Steel-Framed Buildings with Replaceable Energy-Dissipating Fuses. *The 14th World Conference on Earthquake Engineering.* Beijing, China.

Eatherton, M., Hajjar, J. F., Deierlein, G., Ma, X., & Krawinkler, H. (2010). Hybrid Simulation Testing of a Controlled Rocking Steel Braced Frame System. *The 9th U.S. National and 10th Canadian Conference on Earthquake Engineering.* Toronto, Ontario, Canada.

Ekiz, E., & El-Tawil, S. (2008). Restraining Steel Brace Buckling Using a Carbon Fiber-Reinforced Polymer Composite System: Experiments and Computational Simulation. *Journal of Composites for Constructions , 12* (5), 562-569.

Galambos, T. V. (1965). Strength of Round Steel Columns. *Journal of the Structural Division , 91* (ST1), 121-140.

Kalyanaraman, V., Mahadevan, K., & Thairani, V. (1998). Core Loaded Earthquake Resistant Bracing System. *2nd World Conference on Steel in Construction.* San Sabastian, Spain.

Kalyanaraman, V., Mahadevan, K., & Thairani, V. (1998). Core Loaded Earthquake Resistant Bracing System. *Journal of Constructional Steel Research , 46* (1-3), 437-439.

Ma, X., Deierlein, G., Eatherton, M., Krawinkler, H., Hajjar, J., & Takeuchi, T. (2010). Large-Scale Shaking Table Test of Steel Braced Frame with Controlled Rocking and Energy Dissipating Fuses. *The 9th U.S. National and 10th Canadian Conference on Earthquake Engineering.* Toronto, Ontario, Canada.

Mayville, R. A., & Little, A. D. (2001). *Sleeved Column System for Crashworthiness of Light Rail Vehicles.* Final Report, National Research Council, Transportation Research Board.

Mitsuru Sugisawa, F., Hideji Nakamura, I., & Atsuchi Watanabe, M. (1994). *Patent No. 5,471,810.* United States of America.

Mull, N. C. (1999). *Compressive Resistance of Solid Rounds.* Master Thesis, University of Windsor, Department of Civil and Environmental Engineering.

Sennah, K., & Wahba, J. (2004). Compressive Strength of Solid Round Steel Bars. *Journal of Structural Engineering , 130* (1), 147-151.

Sennah, K., Saliba, M., Jaalouk, N., & Wahba, J. (2009). Experimental study on the compressive resistance of stress-relieved solid round steel members. *Journal of Constructional Steel Research , 65* (5), 1034-1042.

Smith, C. V. (1976). On Inelastic Column Buckling. *Engineering Journal , 13* (3), 86-88.

Sridhara, B. N. (1993). *Patent No. 5,175,972.* United States of America.

Timoshenko, S. P., & Gere, J. M. (1961). *Theory of Elastic Stability* (2nd ed.). New York: McGraw-Hill Book Company, Inc.